1-1-1967

Transient stress concentration.

Sharad Kumar
University of Windsor

TRANSIENT STRESS CONCENTRATION

A Thesis
Submitted to the Faculty of Graduate Studies through the
Department of Mechanical Engineering in Partial Fulfilment
of the Requirements for the Degree of
Master of Applied Science at the
University of Windsor

by

Sharad Kumar

Windsor, Ontario
1967

ABE 7038

APPROVED BY: W. North

J. A. Peterman

W. McVinnie

16808

ABSTRACT

This study reports an experimental investigation of stress concentration at a discontinuity in a structural member loaded dynamically.

The geometry considered was a thin rectangular bar of finite width containing a semicircular discontinuity located symmetrically on opposite sides. The experimental procedure involved dynamic photoelasticity with a high intensity microflash and the low modulus urethane model material. The dynamic loading resulted from a falling mass.

The size of the discontinuity and the time after impact were the two parameters considered and the investigation was restricted mainly to the comparison of:

(1) Dynamic and static stress concentration factor

(2) Response of the discontinuity to tensile and compressive impact.

It was found in this case, that the dynamic stress concentration factor was always lower than the corresponding

static value; however, it increases as the discontinuity becomes smaller. The stress concentration factor also increases with time after impact in the range of time considered with a trend indicating an optimum.

It was concluded that in the dynamic case, some of the energy associated with the propagating stress wave was captured by regions of low stress, hence reducing the stress concentration at the critical points.

Little variation was apparent in dynamic stress concentration when the propagating stress wave was tensile or compressive in nature.

ACKNOWLEDGMENT

The guidance, help, and constructive criticism given to me by Dr. W.P.T. North during various stages of this work is sincerely appreciated.

The financial support of the Defence Research Board, Grant Number 1330-02, which made this work possible, is highly valued.

Special thanks is given to Mrs. Jean Deslippe who produced this typescript.

CONTENTS

FIGURES

NOMENCLATURE

c	Velocity of propagation of longitudinal wave, in/sec
E	Static modulus of elasticity, psi
E_d	Dynamic modulus of elasticity, psi
f_σ	Material fringe value, psi-in/fringe (based on shear)
h	Thickness of the model, inch
K	Static stress concentration factor
K_{dyn}	Dynamic stress concentration factor
N	Fringe order
r	Radius of discontinuity, inch
t	Time after impact, millisec
w	Width of the model, inch
ρ	Mass density, lb-sec^2/in^4
σ	Stress, psi
υ	Poisson's ratio

1. INTRODUCTION

1.1 Importance of Dynamic Stress Concentration

Analysis of the behaviour of discontinuities like holes, notches, etc., present in a structure is of fundamental importance. Such discontinuity alters the stress distribution in its neighbourhood so that elementary stress equations no longer describe the state of stress in the structure.

The increasing trend towards higher performances in projectiles and other dynamically loaded structures has made it imperative to know the stress concentration factors and stress distribution at discontinuities. In dynamic loading, the response of these discontinuities is different than in the case of static loading. This is mainly because in impact the action of an external force is not transmitted immediately or invariably to all parts of the member. Deformations and corresponding stresses thus produced are propagated in the form of waves, which react differently than the corresponding statically applied load.

1.2 Scope of this Investigation

The object of the present project was to carry out pre-

liminary investigations on stress concentration factors and stress distribution in a member under dynamic load conditions. The effect of the size of the discontinuity, the time after impact and whether the impulse was tensile or compressive in nature were the main factors considered.

The particular geometry considered here was a thin, finite width plate containing a semicircular discontinuity on both sides. A photoelastic technique of stress analysis was used with the low modulus model material, Hysol 4485.

2. LITERATURE REVIEW

2.1 Stress Concentration

The study of stress concentration has been a field of wide interest, since it gives basic information to the designer about the probable response of irregularities which are inevitable in any design. Many papers have been published which give the value of stress concentration factors under static load conditions found from experimental and theoretical investigations. Research conducted by Coker and Filon (2), Maunsell (19), Neuber (22), Ling (17), Howland (13), Ibrahim and McCallion (14), etc. theoretically and by Wahl and Beeuwkes (28), Frocht (11), etc. experimentally has provided a great deal of useful information on the behaviour of the most common discontinuities under static load conditions. The Engineering Sciences Data Unit of the Royal Aeronautical Society and the Institute of Mechanical Engineers has recently published extensive design data sheets on stress concentration factors (9).

2.2 Dynamic Stress Concentration

With the establishment of the fact that the discontinuities react differently in dynamic loading, it would be of interest

to know their exact reaction in actual practice.

Relatively few investigations have been made in this area because of the complex nature of the problem. So far as the author is aware, the particular geometry of a semicircular groove on either side of a thin rectangular plate has not been analyzed by any worker. However, plates with a circular discontinuity at the centre have been of interest to a few. Pao (24) has theoretically studied the effect of a plane, compressional wave around a circular cavity in an infinitely extended, thin elastic plate. He tackled this problem basically as one of the scattering of stress waves, which, in fact, more closely approximates the phenomenon of vibratory loading. He established that the dynamic stress concentration factors are dependent on the hole size, the incident wave length and Poisson's ratio for the plate material and at certain wavelengths, the stress concentration factors are larger than those encountered under static loading.

Dally and Halblieb (3) studied a similar problem photo-elastically and noted that the dynamic stress concentrations differ significantly from the static stress concentrations and that this difference is dependent on the geometry of the model.

North and Taylor (20) in a similar approach observed that the dynamic stress concentration factors do not experience the very large values characteristic of the static loading conditions. They also noted that the dynamic stress concentration factors varied almost linearly with the ratio of hole diameter to width of the plate. The same effect was observed by Dally and Halblieb (3) as well. It should be noted that Dally and Halblieb (3) and North and Taylor (20) did not consider the effect of incident wavelength or Poisson's ratio.

Shea (26) approached the same problem using strain gauges on thin plexiglass. He concentrated on the effect of pulse wavelength and observed that dynamic concentration factor varies significantly with pulse wavelength. He, however, concluded that the value of dynamic stress concentration factor is significantly lower than the static value.

Flynn (10) and Durelli and Dally (6) also investigated the same problem, but their investigations were of preliminary nature and nothing very significant was observed.

It should be noted that all workers have confined their studies to the effect of compressive loading, hence it was considered of interest to determine the effect of tensile waves in the present study. In one of his recent papers, Davison (5) has suspected a difference in the response of

the material to tensile and compressive loadings respectively. He has attributed this difference toward the possibility of a material changing its properties under the two types of loading. In his paper, he also establishes the criterion for the existence of shock waves.

3. THEORETICAL AND EXPERIMENTAL CONSIDERATIONS

3.1 Stress Wave Propagation

It has been recognized that a dynamic load can create stress waves in a medium. In the event of loading such as that occurring in the present case (a weight falling on a thin, long, rectangular bar), the waves generated are longitudinal (see Appendix C). The velocity of propagation of these stress waves along the bar can be expressed as

$$C = \sqrt{E_d/\rho}$$

where E_d = dynamic modulus of elasticity of the material of the bar,

ρ = mass density of the material,

and C = propagation velocity of a longitudinal wave.

Dally, Riley and Durelli (4) in their paper established that in dynamic photoelasticity, the fringes follow the same law of propagation and reflection as the law for stress waves. They used a rectangular strut subjected to an axial impact to illustrate the potentiality of the method of photoelasticity in visualizing the stress waves in the form of fringes. So the study of stress waves is essentially the study of these photoelastic fringes.

3.2 The Effect of Impact Pulse Duration

The phenomenon of dynamic loading can be divided into three main groups, viz. (a) processes with a quasistatic state of stress, (b) vibrations, and (c) the stress waves (Ref. 26). The time of contact of the falling weight with the body is an important factor in categorizing the process of loading into one of the above groups. Briefly, a quasi-static state of stress would occur if the time of contact during impact is much longer than the time of one free-vibration cycle or the time that a stress wave would take in passing through the body. This state of stress can more closely be approximated by static loading conditions and no real dynamic effect is observed. A state of vibration would occur if the time of contact is the same as the time of one cycle of resonance frequency. Finally, the stress waves are produced only if the time of contact is shorter than the time of one cycle of a free vibration at resonant frequency, which for this material and geometry is about three milli-seconds.

Hence, it is apparent that in order to produce any effective dynamic loading, the time of contact in the process of impact should be much shorter than the time that a stress pulse would take to pass through the body.

3.3 Use of Low Modulus Model Materials

Urethane rubber, commercially known as Hysol 4485 was used as the model material in obtaining birefringent information. Hysol 4485 has an exceptionally low modulus of elasticity of about 500 psi.

Since the velocity of propagation of the stress waves is proportional to the square root of the modulus ($c^2 = E_d/\rho$), such a low value of modulus reduces the velocity in the model to a great extent compared to the conventional, more rigid photoelastic model materials. The low velocity of propagation helps the investigation in two ways:

1. Slow moving fringes can be photographed relatively easily.
2. It takes longer for a stress wave to pass through the body. This makes it possible to satisfy the dynamic loading condition when a falling mass generates the impact load.

Besides this, Hysol 4485 has a very high sensitivity. It exhibits low strain sensitivity so that the time edge effects are negligible.

Hysol 4485, however, suffers from certain undesirable characteristics. It exhibits pronounced deviation from linearity in stress-strain relation at higher stress level.

Like many other photoelastic materials, its viscoelastic behaviour is prominent. Finally, Hysol 4485 has relatively poor machinability.

3.4 Dynamic Stress Concentration Factors

In this report, the dynamic stress concentration factor has been defined as

$$K_d(t) = \frac{\sigma^d_{max}(t)}{\sigma^d_{nom}(t)} \qquad (1)$$

where $\sigma^d_{max}(t)$ = the maximum dynamic stress at the boundary of discontinuity as a function of time, and

$\sigma^d_{nom}(t)$ = the stress that would occur at the same instant and position if no discontinuity existed.

By making the assumption that the stress waves are only longitudinal in the present investigation (see Appendix C), and applying the stress optic law (Appendix E), equation (1) can be reduced to

$$K_d(t) = \frac{f_{\sigma\ max}(t) \times N_{max}(t)}{f_{\sigma\ nom}(t) \times N_{nom}(t)} \qquad (2)$$

where $f_{\sigma\ max}(t)$ = the maximum stress optical coefficient,

$f_{\sigma\ nom}(t)$ = the nominal stress optical coefficient,

$N_{max}(t)$ = the maximum fringe order obtained at the boundary of discontinuity, and

$N_{nom}(t)$ = the fringe order at the same position and time if no discontinuity existed.

Dally, Durelli and Riley (4) observed that for Hysol 4485 for a large range of strain rate (8 in/in-sec to 65 in/in-sec) $f_{\sigma\ max}(t)$ is equal to $f_{\sigma\ nom}(t)$ for all values of t. In the present investigation, the strain rate had been estimated as about 17 in/in-sec. This reduces equation (2) to

$$K_d(t) = \frac{N_{max}(t)}{N_{nom}(t)} \qquad (3)$$

It should be noted that the conventional definition of stress concentration factor is different than the one given above. It is generally defined as

$$K = \frac{\sigma_{max}}{\sigma_{nom}}$$

where σ_{nom} is calculated by using the net area of cross-section at the position of the discontinuity.

4. OUTLINE OF EXPERIMENTAL PROCEDURE

4.1 Particular Problem Studied

The problem involved studying the effect of tensile dynamic loading on stress concentration factors at a discontinuity. The discontinuities were in the form of semi-circular notches on both the sides of the model. Hysol 4485, Urethane rubber was used as the model material.

Loading was accomplished by dropping a guided steel weight of 1-1/2 ounces a distance of 40 inches onto the top of the load-cell which, in turn, loaded the model in tension. (See figures 1 and 2.)

4.2 Description of the models

The models were machined from a 1/4 inch thick Urethane rubber sheet. The geometric details of the models tested are shown in figure 3.

4.3 Technique of Recording the Phenomenon

The repeatability technique was used to record the birefringent information. The main requisites for this technique, besides a conventional polariscope, are a still camera, a light source which must give a single flash of high intensity

and short duration, a triggering device synchronized with the event and a delay circuit. This works as follows:

a. The event begins when a steel weight is released from its elevated position.

b. The falling weight trips a photoelectric trigger that monitors the time delay.

c. The weight impacts the load cell on the model and the fringes begin propagating the length of the model. This impact also triggers the time delay circuit.

d. The output from the time delay circuit triggers the light source and thus a photograph is recorded at a predetermined time as given by the time delay circuit.

e. The repetition of the same procedure for different delay times gives a series of photographs, describing the entire event.

It should be noted that the camera is left wide open throughout each cycle and the light source acts as its own shutter. (See figure 1.)

In this investigation, the falling weight initiates the triggering pulse by shorting an electrical contact while striking the load cell. Although a fine delay unit was

assembled in the University Research shop, the incorporated delay circuit of a Tektronix 555 oscilloscope was found more reliable and easier to handle, and it was used to delay the pulse throughout the study.

This delayed output from the oscilloscope externally triggered the light source. The light source used was a high intensity stroboscope, which provides a light pulse of about 10 microseconds duration (Appendix D). In this time interval, the longitudinal wave moves approximately .033 inches and the action is effectively stopped.

Type 47 polaroid film, which has a very high speed rating of 3000 ASA was used. The description of the complete equipment used is given in Appendix D.

The repeatability technique of recording the birefringence information is probably the best, since it gives large, accurate, full-field photographs. The high degree of repeatability demonstrated in figure 4 shows the potential of the method.

5. RESULTS AND DISCUSSION

5.1 Birefringence Photographs

5.1.1 Birefringence Photographs Showing Fringe Propagation in a Model Without Discontinuity - Figure 5 is a series of birefringent photographs showing the propagation of fringes in a model without discontinuity. The models were loaded in tensile impact initiated at the bottom of the photograph. Photograph 1 shows the no-load condition. The following should be noted:

a. A-A is the position of the centreline of all discontinuities of different sizes.

b. B and C are the fringes due to clamping stresses and should not be mistaken as loading stress.

c. All irregular dark and light spots, such as D, are due to uneven distribution of light around the filament of the light source.

d. Dark edges on both the sides of the model show the poor machinability of Urethane rubber; also, since the light field is not parallel, boundary definition is not good.

The half-order fringe can be seen in photograph 2 of figure 5. Warping of the plane section of the bar is suggested by the prominent curvature shown by this half-order fringe. The 1.5 order fringe is almost straight and the 2.5 order fringe, which appears in photograph 7, is straight or slightly curved in the opposite direction. This phenomenon was expected and has been justified theoretically by Jones and Ellis (15) as a result of the development of a two dimensional state of stress. An inspection of photographs from 2 to 7, however, shows that the fringes have a tendency to reduce their curvature as they propagate. This effect, however, has not been considered when describing the stress concentration factor which was defined for uniaxial stress. (Sec. 3.1.1.)

It can be confirmed from these photographs that fringes of different order move at different but almost constant velocities. Velocity of the half-order fringe was determined as 3250 inches per second. It is worth mentioning here that Dally, Riley, and Durelli (4) found the half-order fringe velocity to be as high as 3420 inch/sec in the same material - Urethane rubber. Since the velocity of propagation is a function of the material properties like modulus of elasticity and density, it suggests that the material properties vary from lot to lot to an appreciable extent. Figure A-2 of

Appendix A shows the velocity of each fringe order as determined in this investigation.

5.1.2 Wave Propagation Through the Discontinuity - Figure 6 presents a series of photographs showing the wave propagation through the discontinuity for a r/w ratio of 0.156. Photograph 1 of figure 6 again shows the no-load condition and the tensile impact is initiated at the bottom of the photograph.

A slight increase of the fringe order at the discontinuity in photograph 2 suggests that the wavefront has arrived at the discontinuity, although the half-order fringe is quite far from the discontinuity. This suggests that the pulse wavelength is very long.

An inspection of photographs 6, 7 and 8 gives an impression that the half-order fringe (or the lower stress) has a tendency to stick to the discontinuity (photographs 6 and 7) until the 1.5 order fringe (higher stress) pushes it out the narrower section, such that the area A in photograph 8 is completely and suddenly occupied by a higher order fringe. This observation suggests a kind of forced propagation of waves in the bar.

Figure 7 shows a relation between time and distance traversed by the half-order fringe, measured from the photo-

graphs of figure 6. The datum of the measurements was a point about 0.9 inch below the centreline of the discontinuity. The half-order fringe arrives at this point 1.5 milliseconds after the impact.

The slope of this curve at any point, therefore, gives the velocity of half-order fringe at that moment.

Three different zones A, B, and C of the curve are apparent. Lines ab and cd represent the lower and the upper boundaries of the discontinuity respectively.

The linear portion OE of the curve in zone A shows the smooth upbound motion of the wave with almost constant velocity. Beginning at point E, the slope of the line decreases rapidly, suggesting a very low wave velocity in zone B. In zone C, this trend reverses and the slope reaches a terminal value that is approximately 35 per cent greater than that in zone A.

It should be noted that zone B starts at a point a little lower than the beginning of the discontinuity and extends to about 20 per cent of the span of the hole.

It appears that an analogy can be established between the fringe propagation through the discontinuity and the fluid flow through a constriction.

Velocity of flow goes down at a point just before the entrance to the nozzle and keeps falling down to a point a little after the entrance, forming a similar zone B. After that, the velocity shoots up according to the change in area of cross-section, forming something similar to zone C of our case.

5.2 Graphic Interpretation of Photoelastic Data Obtained from the Birefringent Information

5.2.1 Stress Distribution Around the Discontinuity -

Figure 8 shows the distribution of stress around one inch diameter discontinuity 3.5 milliseconds after impact. The highest fringe order of 9.6 fringes was found at the centre of the hole ($\theta = 0^\circ$). To compare this stress distribution under dynamic loading to that under static loading, the same model was loaded to 9.6 fringes under static tensile loading, and this stress distribution is also shown in figure 8.

An inspection of figure 8 shows that at θ close to 90°, the associated stresses in the dynamic case are higher than in the static case. This observation probably reveals the significant difference between dynamic and static loadings. It is entirely possible, indeed probable, that in the dynamic case, some of the energy associated with the wavefront is captured by the corners, which is impossible under normal

static conditions.

5.2.2 Maximum Fringe Order as a Function of Time - Figure 9 shows the effect of the time after impact on maximum fringe order at the discontinuity.

5.2.3 Effect of Time after Impact on Stress Concentration Factor - Figure 10 shows the variation of stress concentration factor with time lapse after impact. It should be noted that dynamic stress concentration factor is always lower than the static stress concentration factor in the entire range studied. This difference between the stress concentration factors varies from 15 per cent to 50 per cent - depending upon the time after impact. This effect has been observed by many workers (Ref. 3, 12, 21, 26) but could not be explained very satisfactorily. The interesting result mentioned in section 5.2.1 may probably explain this behaviour. It was expected that some of the energy associated with wavefront gets captured by the corners and because a part of the energy is so removed to an area of low stress, it is reasonable to expect lower stress concentration.

It should also be noted that dynamic stress concentration factor is time dependent. The same effect was observed by Dally and Halblieb (3) and North and Taylor (21); although theoretically Pao (24) showed that dynamic stress concentra-

tion depends only on size of the discontinuity, impulse wavelength and Poisson's ratio. Both of these latter parameters are constant here.

The trend towards increasing stress concentration as the time after impact increases, however, seems to be reasonable and can be explained. Although no actual measurements were made to record the pulse shape, figure 11, which has been taken from an investigation by Clark (1) would suffice to give the explanation. The wavefront has relatively low energy associated with it. As the wavefront reaches the discontinuity, the part of the energy associated with it which is captured by the low stress area, forms an appreciable fraction of the total energy. Now, as the latter part of the stress pulse approaches the discontinuity, little or no energy is captured by the corners since they are already stressed, thus increasing the concentration at the critical area progressively. This would obviously give rise to progressively higher stress concentration factors till the peak of the pulse reaches the position of the discontinuity. If the study were extended to a longer period after impact, it should be expected that the stress concentration factor would tend to decrease as the trailing part of the pulse passes through the discontinuity. From the curves in figure 10, this maximum trend is evident, although not completely established.

5.2.4 Dynamic Stress Concentration Factor as a Function of r/w Ratio - Figure 12 shows the effect of the size of discontinuity on stress concentration factor. Values of static stress concentration factor have been obtained from Peterson (25).

Figure 13 shows the curves giving per cent decrease of dynamic stress concentration factor over the corresponding static value for various hole ratios. A well defined minima can be noticed in every curve. The difference in the two values decreases for low values of r/w ratios and then increases rapidly.

It appears that the net effect of the following two factors is responsible for this behaviour. Firstly, the deflection of the energy in the low stress area. This effect would tend to decrease the stress level. Secondly, the reduction of the area at the discontinuity, which tends to increase the stress level.

The initial portion of the curve suggests that the former factor is gradually losing its effect with the increase in r/w ratio until its value reaches about 0.2. At this point, the size of the discontinuity starts getting so large that the wavefront tends to see it as more of an infinite surface and reflects from it, thus reducing the boundary stress.

An attempt was made to correlate the dynamic stress concentration factor to the hole ratio by a mathematical expression. The following empirical equation for the dynamic stress concentration at 2.2 milliseconds after impact gives values agreeing approximately with the test results (see figure 12).

$$K_{dyn} = 1.615 + 3.301\ (r/w) + 17.767\ (r/w)^2 - 64.097\ (r/w)^3$$

$$(0.08 < r/w < 0.26)$$

Wahl and Beeuwkes (28) found a similar equation[1] for the static stress concentration factor as

$$K = 2.75 + 1.28\ (r/w)^2 + 8.00\ (r/w)^3$$

5.2.5 Comparison of Dynamic Stress Concentration Factors under Tensile and Compressive Impact - A model with r/w ratio of 0.156 was tested for compression impact also. Dynamic stress concentration factor as determined in this case is given in figures 14 and 15 as a function of time and compared with the results of tension impact.

It is apparent that dynamic stress concentration factor under tensile and compressive loading is equivalent until about 2 milliseconds after impact, after which the concentration factor obtained under compression impact is lower than

---

1 This equation has been modified according to the changed definition of stress concentration factor used here. The actual equation given by Wahl and Beeuwkes (28) is

$$K = 2.75 - 2.75\ d/w + 0.32\ (d/w)^2 + 0.68\ (d/w)^3$$

that obtained under tension impact.

It is quite probable that the tensile properties of the material may be different from the compressive properties which may give rise to the difference in wave propagation. It should be noted, however, that a difference of only two per cent was found between the values of concentration factors under tension and compression, which may be attributed to experimental error. Although every effort was made to have the same physical arrangement of loading in both cases, it was found hard to load the model in compression because of its flexibility.

Davison (5) established, by purely theoretical considerations, that a condition of shock prevails when the wave speed increases upon the passage of the disturbance and centred simple waves prevail when the wave speed decreases upon the passage of the disturbance. It was observed that the velocity of fringe propagation increases when it passes through the major portion of the discontinuity (see section 5.1.2 - chapter 5). Figure 7 shows an increase of approximately 35 per cent in the fringe velocity while passing through zone C. Thus, it can rightly be suspected that it is a condition of shock that is being observed in zone C of the model. However, Davison showed that the necessary condition for such a situation is that the material be "hardening" in tension. It is possible that the

material used behaves as a hardening material in dynamic loading at high strain rate, although no experiment was or could be executed with the existing apparatus to test this. The static ttsts for the material indicate that it is not a hardening material; however, the viscoelastic nature of this material precludes the assumption that this is still true at higher strain rates.

5.3 Optimum Design Criteria

If one calculates the maximum stress at this type of discontinuity theoretically, assuming that all of the potential energy of the falling weight is absorbed in the model elastically, and that the static stress concentration factors are representative, then the design in this material would certainly be conservative, i.e. this theory gives a stress that is at least 80 per cent higher than actually exists (see Appendix B). In many situations, this is acceptable since an experimental program is not possible or economical; however, when cost and particularly weight considerations are important, then this approximate answer is unacceptable, particularly if 45 per cent of the area can be removed, thus reducing the weight. Similarly, employing a simplified stress wave propagation theory (see Appendix C) and corresponding static stress concentration factor, the result is some 280 per cent conservative.

5.4 Experimental Error - Estimation

Although no actual calculations can be made to determine the experimental errors, the following has been estimated after various trials:

a. Repeatability of the Experiment

It is estimated that the whole experiment can be repeated within a range of ± 5 per cent. This high repeatability can be attributed towards the use of precision controls and a reliable technique of recording the phenomenon.

b. Interpretation of the Information

It is estimated that the interpretation of the birefringent information can involve an error as high as ± 15 per cent. This is because of poor photographs resulting from the use of the low intensity, nonmonochromatic, relatively long duration light pulse.

6 RECOMMENDATION FOR FUTURE WORK AND IMPROVEMENTS

6.1 Suggestions for Future Work

(1) Since it has been recognized that dynamic stress concentration factor is dependent on pulse wavelength, Poisson's ratio and the time after impact, an extensive study should be conducted involving all the above parameters.

(2) The semicircular discontinuity provides sharp corners that form the region of low stress. It was found that a part of the energy of the propagating disturbance gets captured by this low stress area. Different behaviour should be expected from a discontinuity which does not provide a similar low stress region. It would, therefore, be of interest to study the behaviour of discontinuities of other than a semicircular nature.

(3) Models of different width should be used to make the study more general.

(4) Use of more than one model material is recommended since it is suspected that the material properties in tension may be different from its properties in compression.

(5) Model material should be completely calibrated dynamically for stress and strain optical coefficients and modulus of elasticity.

6.2 Suggestions for Improvements

(1) Improvements must be made in the present setup for producing tension impact such as:

(i) Some stiffer material should replace bakelite for the load cell. Magnesium can make a good substitute.

(ii) The motion of the load cell should be guided to prevent it from side swaying.

(2) Since a stress pulse of shorter wavelength is desirable, it is suggested that loading by an exploding charge or by a propagating missile be considered.

(3) Efforts should be made to have accurate measurements of

(i) duration of impact, and

(ii) variation of applied load with time.

This would assist in having a comparatively clear view of the whole phenomenon.

(4) The low intensity of the light obtained from the stroboscope made it impossible to use monochromatic light. This has resulted in the poor birefringent photographs. A ruby laser can be an ideal substitute for light source here, since its output has almost all the desirable qualities for use in dynamic work; namely, highly intense, monochromatic, polarized, parallel and a very short duration of light pulse.

7 CONCLUSIONS

(1) Dynamic stress concentration factor, as determined in this study and in the region of r/w ratio tested, is always lower than the corresponding static value, insome cases from 15 per cent to 50 per cent less than the static value depending on the time after impact.

(2) The difference between dynamic and static concentration factors diverges rapidly for large r/w ratios. It appears that the wavefront tends to see the increasing size of discontinuity as more of an infinite surface, thus reflecting from it and reducing the boundary stress.

(3) Dynamic stress concentration factor depends significantly on the time after impact. It was found to vary almost linearly from 1.7 milliseconds to 2.1 milliseconds. After 2.1 milliseconds of impact, it was almost constant for higher values of r/w ratio. For the r/w ratio of 0.093, however, it had a tendency to increase throughout the time span considered (1.7 milliseconds to 2.3 milliseconds).

(4) Little difference is apparent in stress concentration for a tensile and compressive dynamic load.

(5) It was found that in case of impact, a part of the

energy gets captured by the region of low stress, thus lowering the stress concentration at the critical points and therefore it would appear that streamlining the discontinuity would not improve the stress concentration in the dynamic case as much as it does in the static case.

(6) The theoretical estimation of the maximum stress induced during the impact yields a value which is at least 80 per cent higher than actually exists (see Appendix B).

(7) In general design problems, it would appear that the use of the recorded values for static stress concentration factor will give conservative results when dynamic loads are encountered.

BIBLIOGRAPHY

1. Clark, A.B.J. "Static and Dynamic Calibration of a Photoelastic Model Material, CR-39," S.E.S.A. Proceedings, XIV (NO.1), 195-204.

2. Coker, E.G., and L.N.G. Filon. Photoelasticity, Cambridge: Cambridge University Press, 1931.

3. Dally, J.W. and W.F. Halbleib. "Dynamic Stress Concentrations at Circular Holes in Struts," The Journal of Mechanical Engineering Science, March, 1965

4. Dally, J.W., W.F. Riley, and A.J. Durelli. "A Photoelastic Approach to Transient Stress Problems Employing Low-Modulus Materials," Journal of Applied Mechanics, Trans. A.S.M.E., December, 1959, 613-620.

5. Davison, L. "Propagation of Plane Waves of Finite Amplitude in Elastic Solids," J. Mech. Phys. Solids, XIV (1966) 249-270.

6. Durelli, A.J. and J.W. Dally. "Stress Concentration Factors under Dynamic Loading Conditions," Journal of Mechanical Engineering Science, I (NO.1, June 1959), 1.

7. Durelli, A.J. and W.F. Riley Introduction to Photomechanics, Englenwood Cliffs, N.J., Prentice-Hall, Inc., 1965.

8. Durelli, A.J. and W.F. Riley. "Stress Distribution on the Boundary of a Circular Hole in a Large Plate During Passage of a Stress Pulse of Long Duration," Journal of Applied Mechanics, Trans. A.S.M.E., (June, 1961), 245-251.

9. Engineering Sciences Data Unit, Stress Concentration Data, No. 65004, London: Engineering Sciences Data Unit, Inst. Mech. Engrs., 1965.

10. Flynn, I.D. "Studies in Dynamic Photoelasticity," Ph.D. thesis, Illinois Institute of Technology, 1954.

11. Frocht, M.M. "Factors of Stress Concentration Determined by Photoelasticity," Journal of Applied Mechanics, Trans. A.S.M.E.

12. Halbleib, W.F. "The Experimental Determination of the Stress Concentration Factors at the Boundary of a Central Circular Hole with Both Soft and Rigid Struts Having Various Hole Diameters to Width Ratios when Subjected to Longitudinal Dynamic Impact Loads," Ph.D. thesis, Cornell University, 1961.

13. Howland, R.C.J. "On the Stresses in the Neighbourhood of a Circular Hole in a Strip Under Tension," Proc. Royal Society, 1930, (A229), 49.

14. Ibrahim, S.M. and H. McCallion. "Elastic Stress Concentration Factors in Finite Plates Under Tensile Loads," Journal of Strain Analysis, I (No. 4, 1966), 306-311.

15. Jones, O.E. and A.T. Ellis, "Longitudinal Strain Pulse Propagation in Wide Rectangular Bar-Part I,II," Journal of Applied Mechanics, Trans. A.S.M.E., I (No. 4, March 1963), 51-69.

16. Kuske, Albrech. "Photoelastic Research on Dynamic Stresses," Experimental Mechanics, VI (NO. 2, Feb. 1966) 105-112.

17. Ling, C.B. "Stress in a Notched Strip Under Tension," Journal of Applied Mechanics, Trans. A.S.M.E., XIV (No. 4, Dec. 1947) 275.

18. Lubahn, J.D. "Comparison of Methods of Determining Stress Concentration Factors," S.E.S.A. Proceedings, XVI (No. 2), 139-144.

19. Maunsell, F.G. "Stress in a Notched Plate Under Tension," Philosophical Magazine, XXI (1936), 765.

20. North, W.P.T., and C.E. Taylor. "Dynamic Stress Concentration Using Photoelasticity and Laser Light Source," Experimental Mechanics, XVI (No. 7, July 1966) 337.

21. North, W.P.T. "A Laser Light Source in Dynamic Photoelasticity," Ph.D. thesis, TAM department, University of Illinois, Urbana, 1965.

22. Neuber, H. "Theory of Notch Stresses: Principles for Exact Stress Calculation," Julius Springer, Berlin, 1937. Translated by F.A. Raven, David Taylor, Model Basin, Washington, D.C., Nov. 1945.

23. Ozane, J. "Strain Calibration in Dynamic Photoelasticity," Master's thesis, TAM department, University of Illinois, Urbana, 1965.

24. Pao, Y.H. "Dynamical Stress Concentration in an Elastic Plate," Journal of Applied Mechanics, Trans. A.S.M.E. XXIX (No. 2, June, 1962), 299-305.

25. Peterson, R.E. Stress Concentration Design Factors, New York: John Wiley and Sons, Inc.

26. Shea, Richard. "Dynamic Stress Concentration Factors," Experimental Mechanics, (January, 1964), 20-24.

27. Stein, K.O. "Dynamic Photoelasticity-A critical Review and Experimental Study," Master's thesis, TAM department, University of Illinois, Urbana, 1963.

28. Wahl, A.M. and Beeuwkes, R., Jr. "Stress Concentration Produced by Holes and Notches," Trans. A.S.M.E. LVI (1934), 617-625.

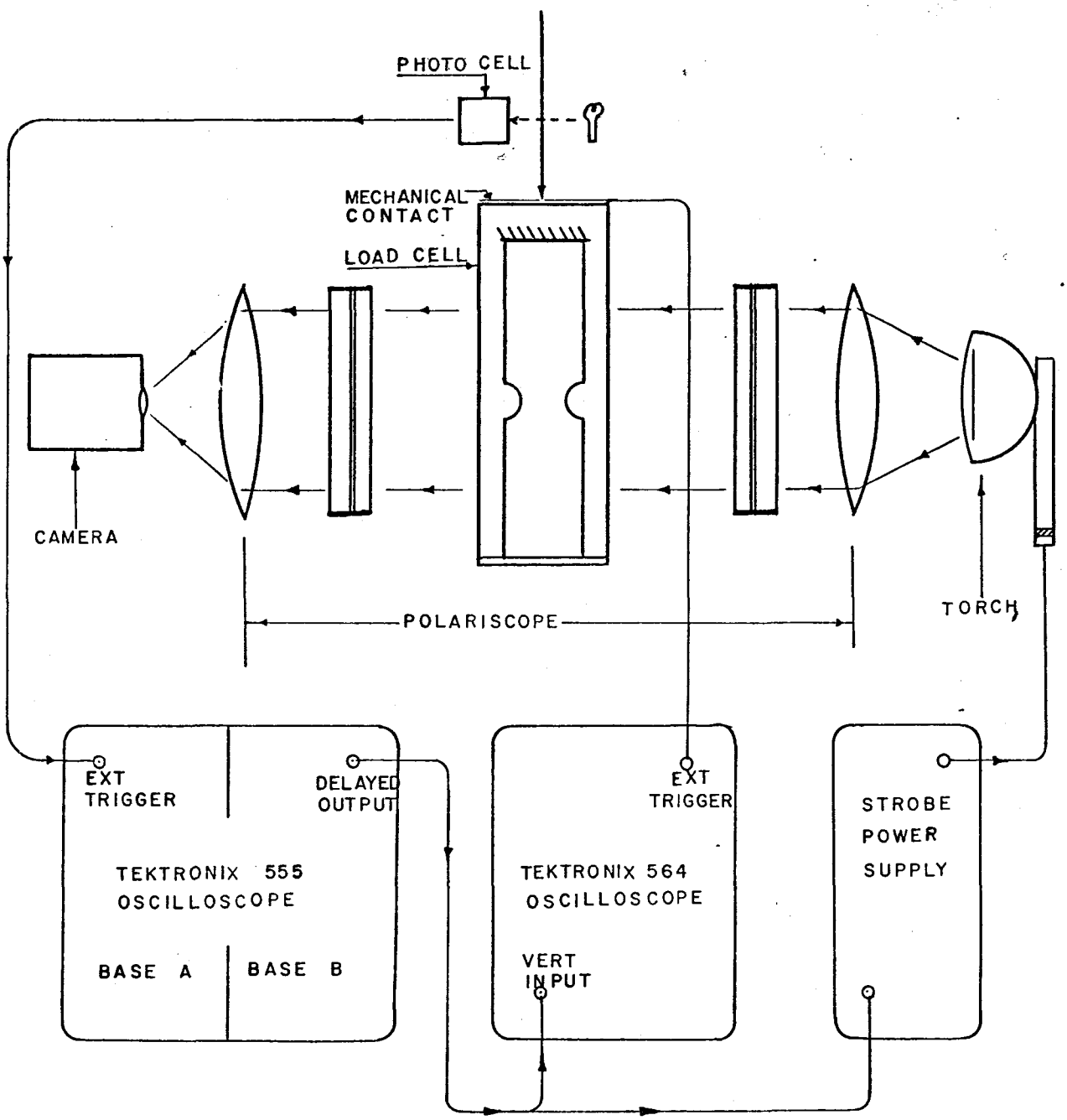

Figure 1 - Block diagram of the experimental arrangement

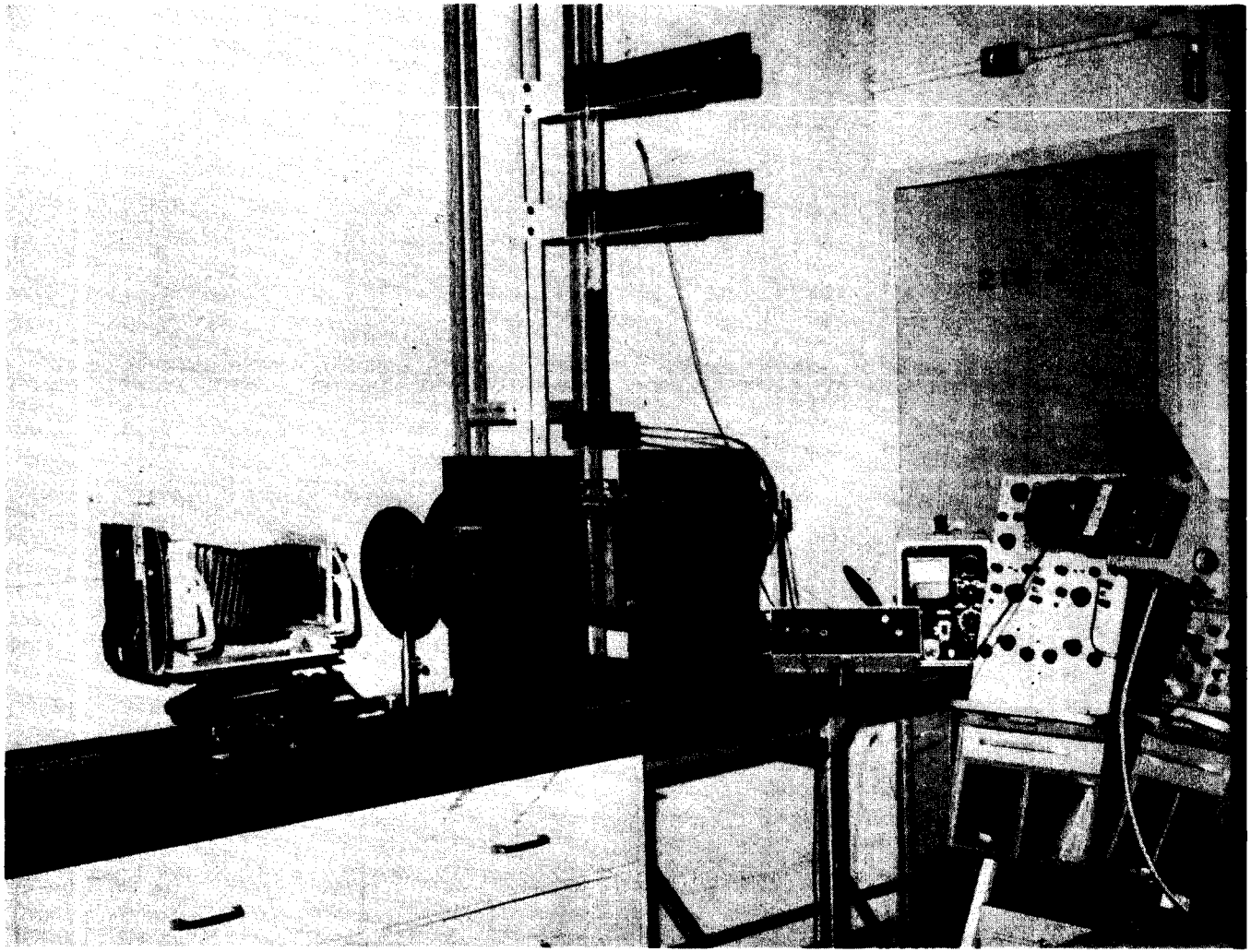

FIGURE 2 - PHOTOGRAPH OF LABORATORY EQUIPMENT

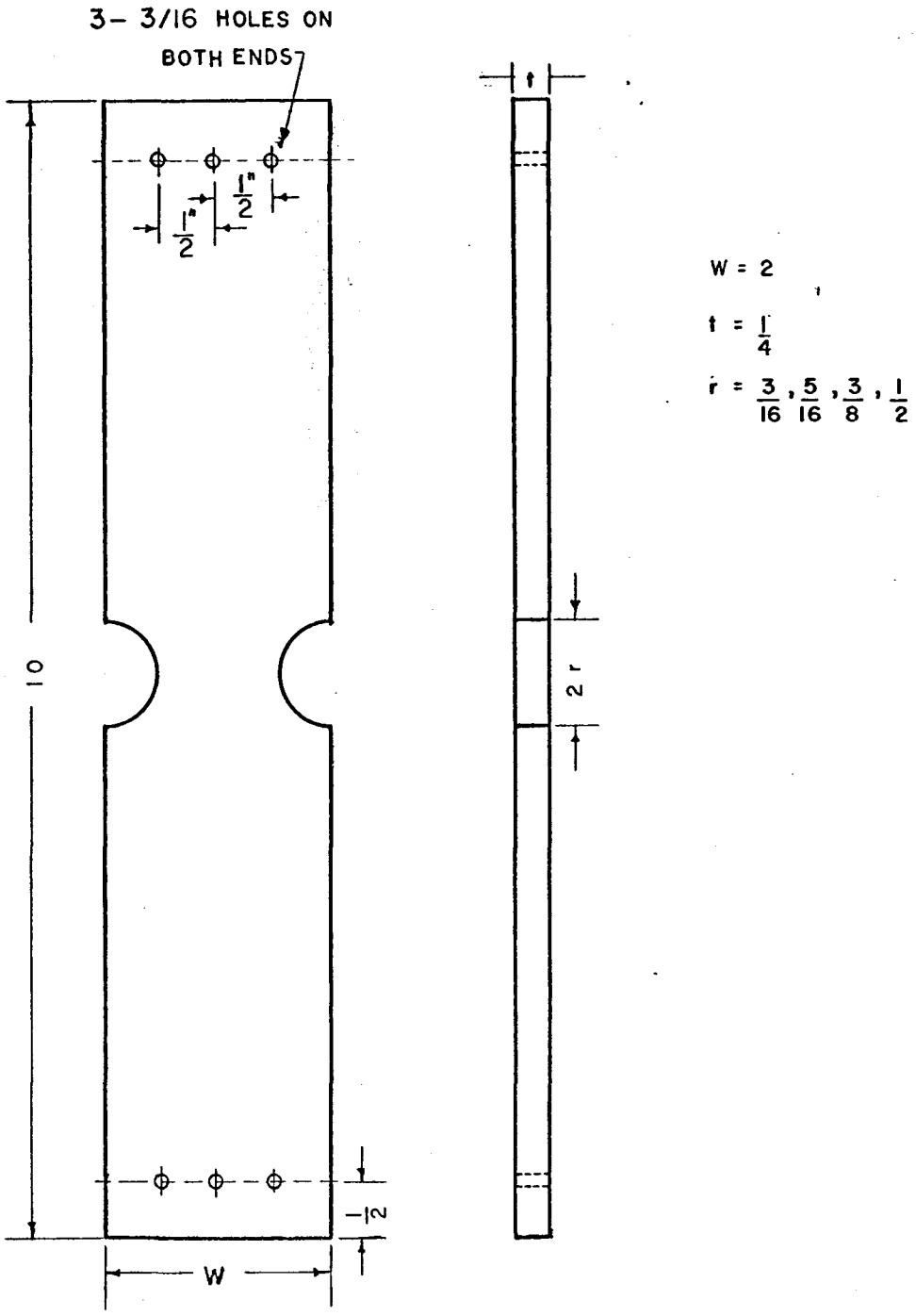

Figure 3 - Dimensions of the models used

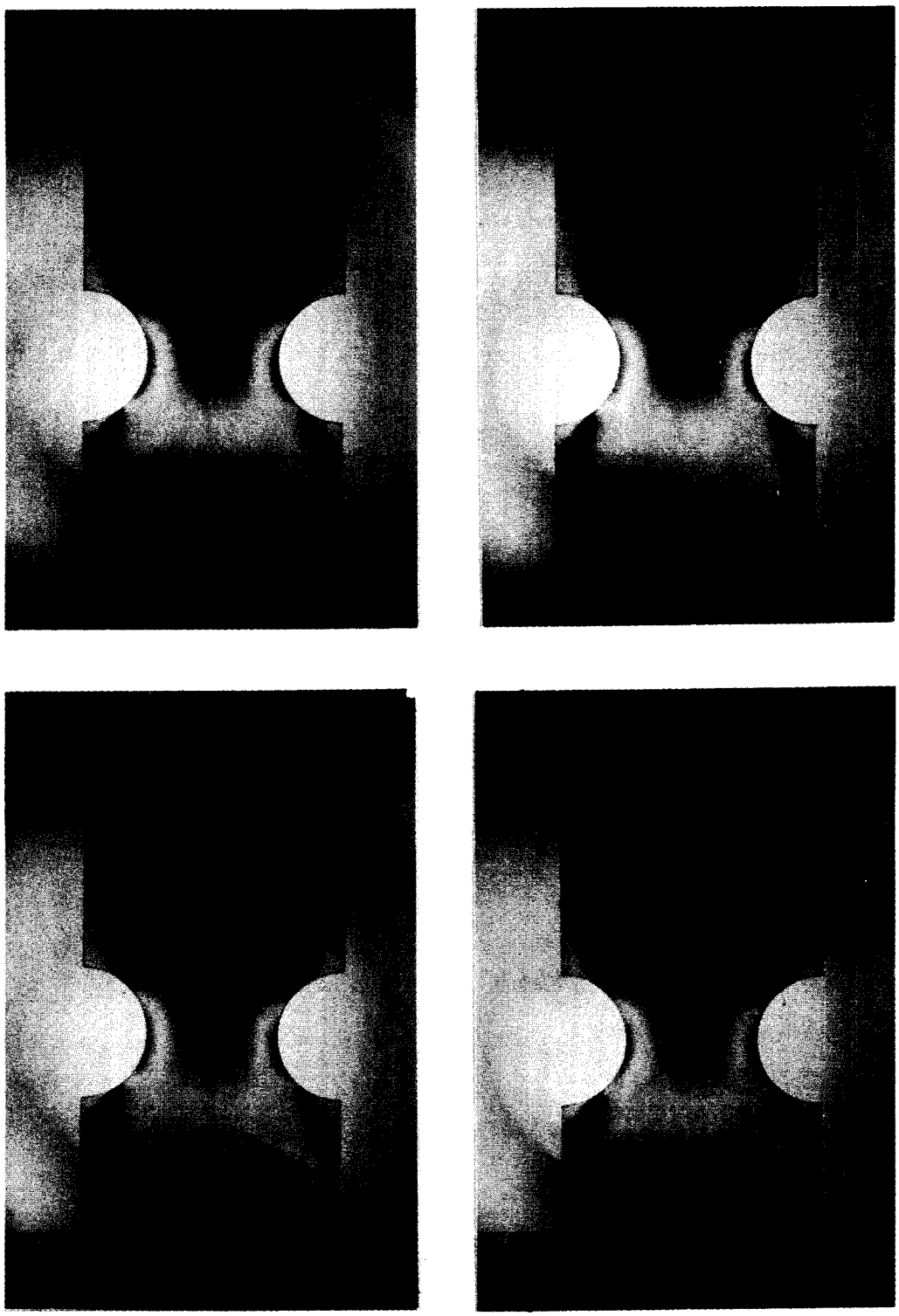

Figure 4 - Repeatability test
Time after impact - 1.7 milliseconds
r/w - 0.25

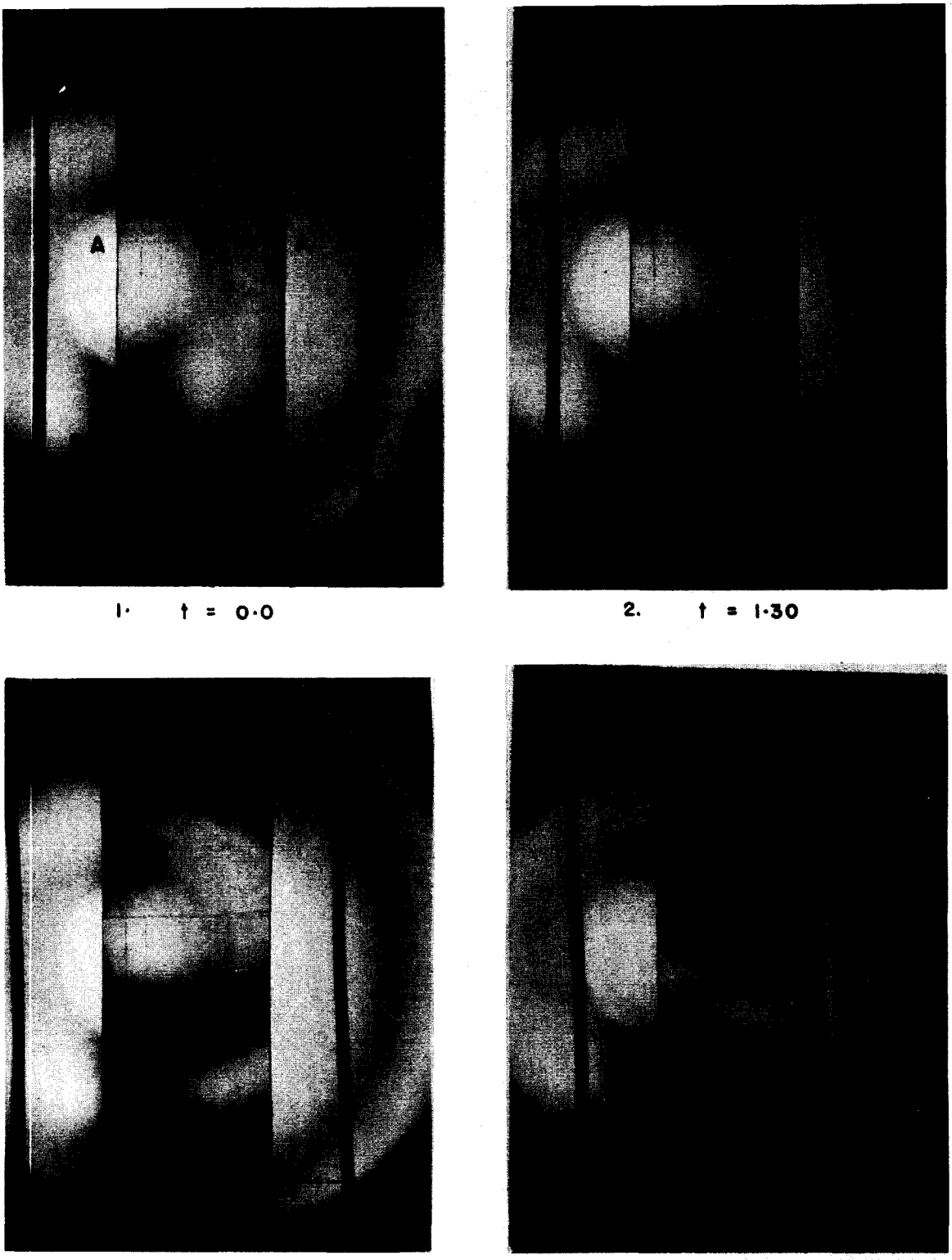

Figure 5 – Birefringence photographs showing the wave propagation in a model without any discontinuity

5. t = 1.90

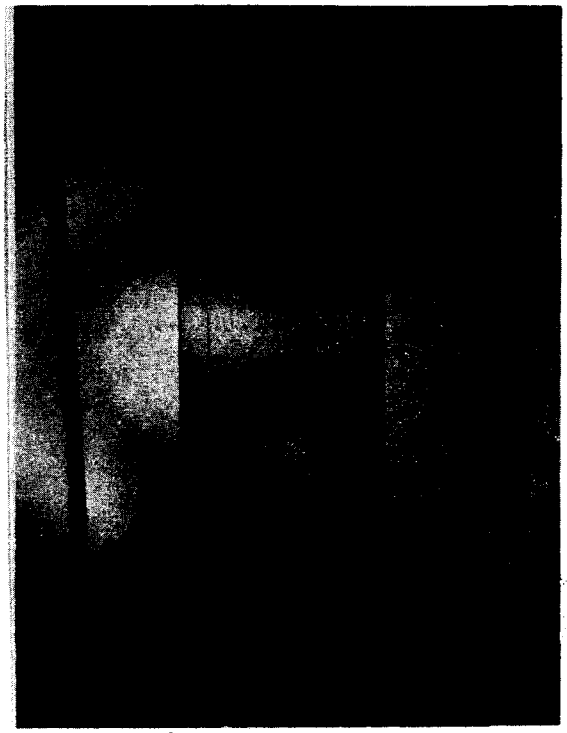

6. t = 2.00

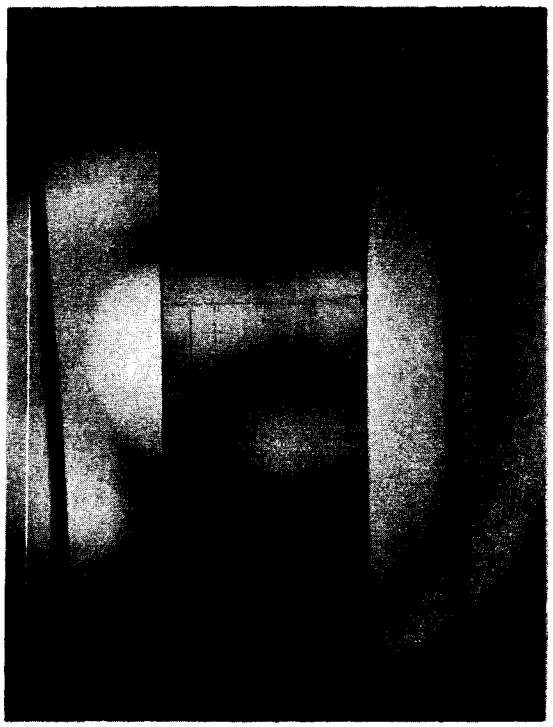

7. t = 2.10

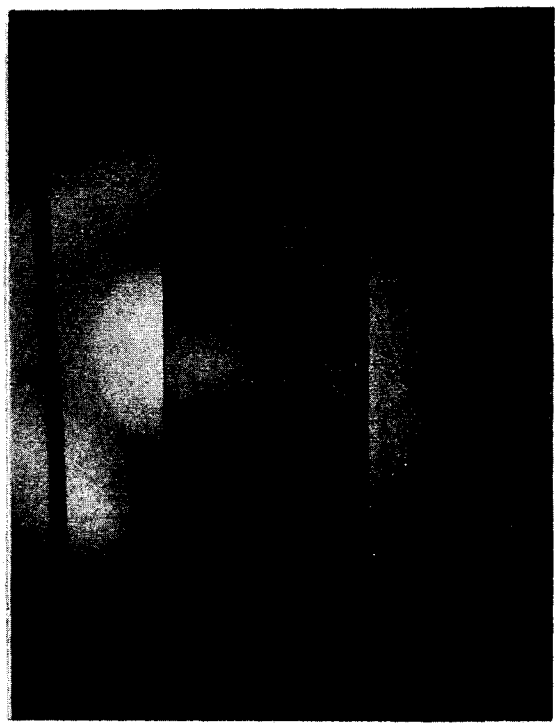

8. t = 2.25

Figure 5 (continued)

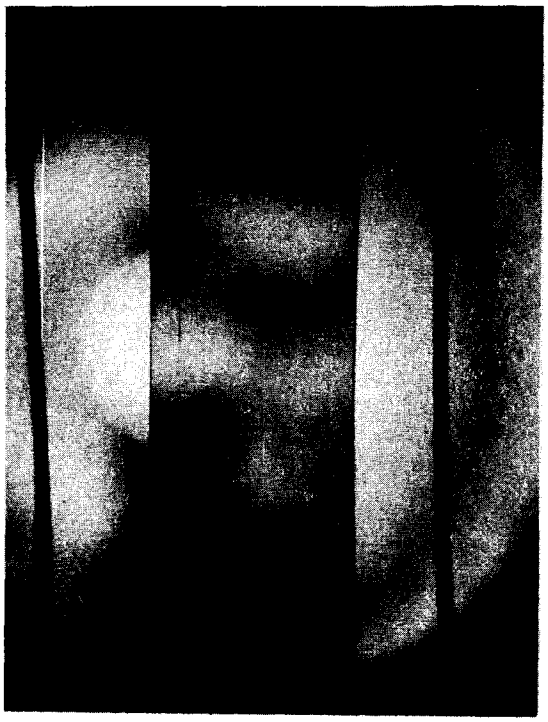

9. t = 2.30

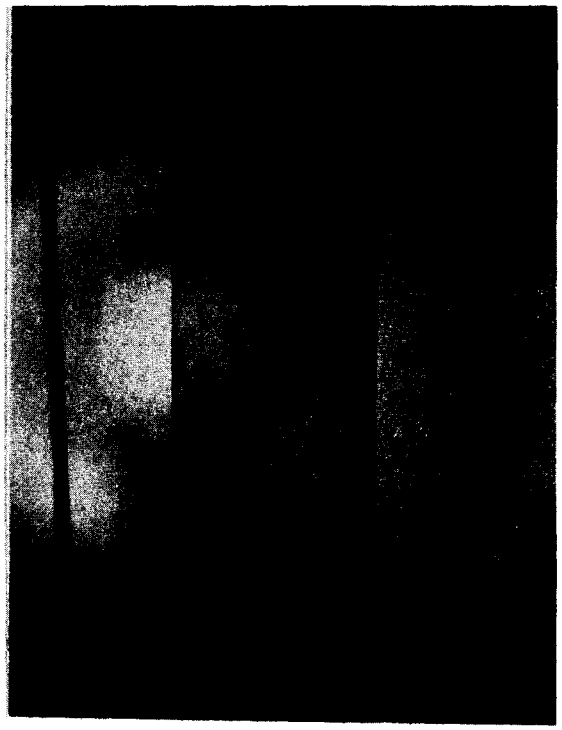

10. t = 2.60

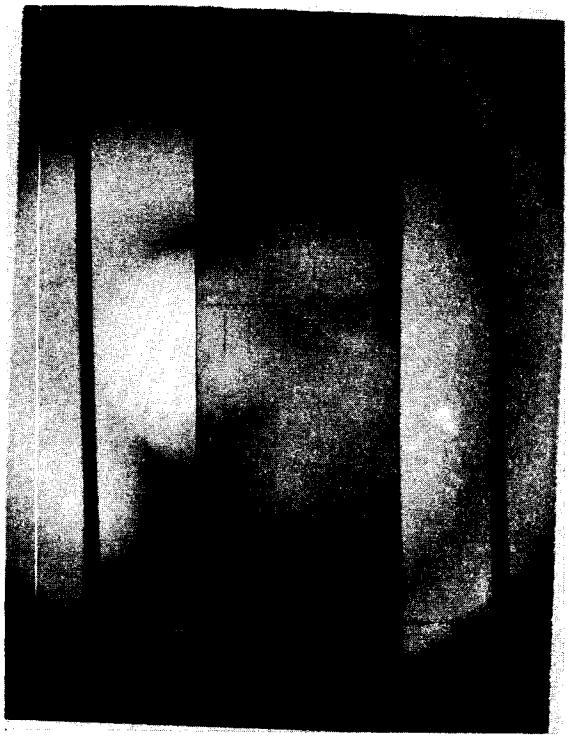

11. t = 2.75

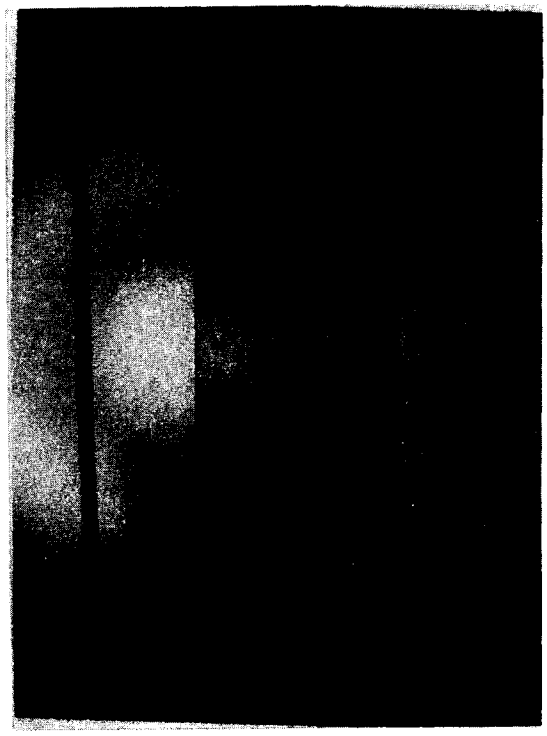

12. t = 2.85

Figure 5 (continued)

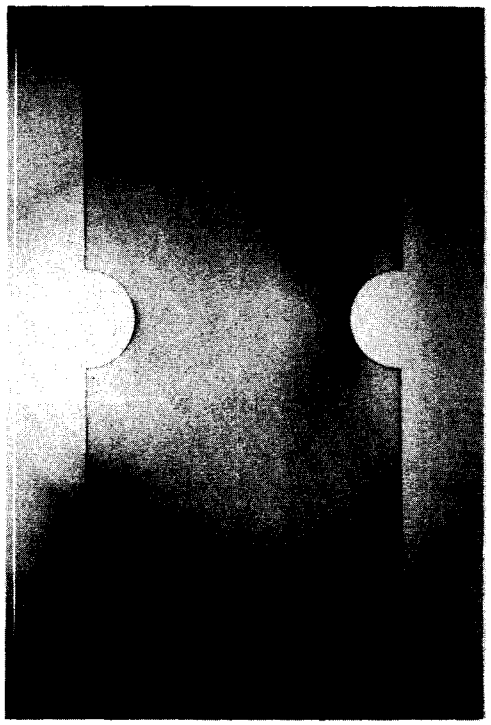

1. t = 0.0

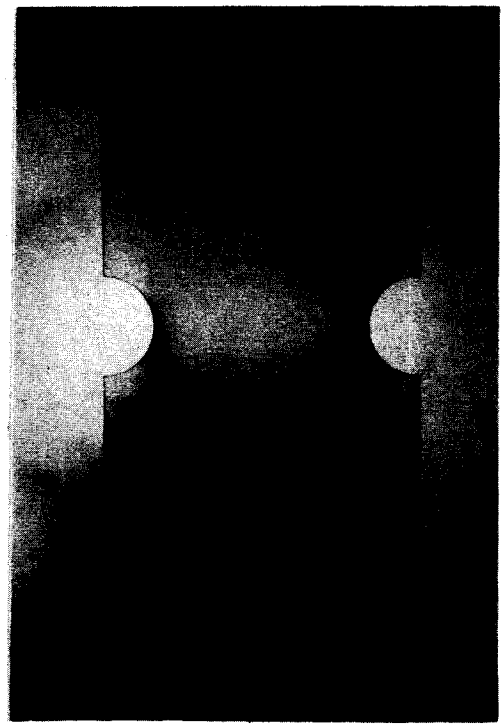

2. t = 1.5

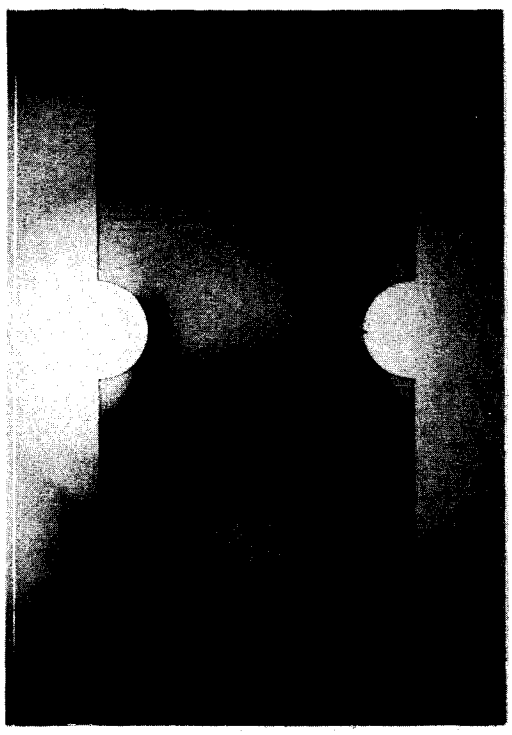

3. t = 1.6

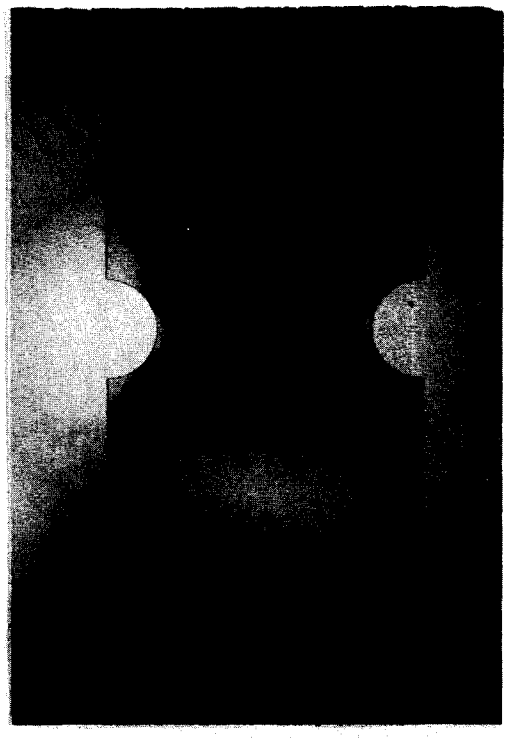

4. t = 1.7

Figure 6 – Development of dynamic birefringence for r/w = 0.156

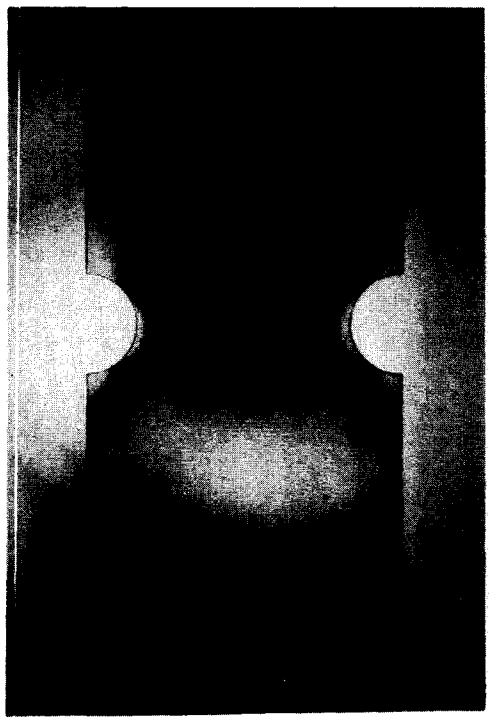

5. t = 1.8

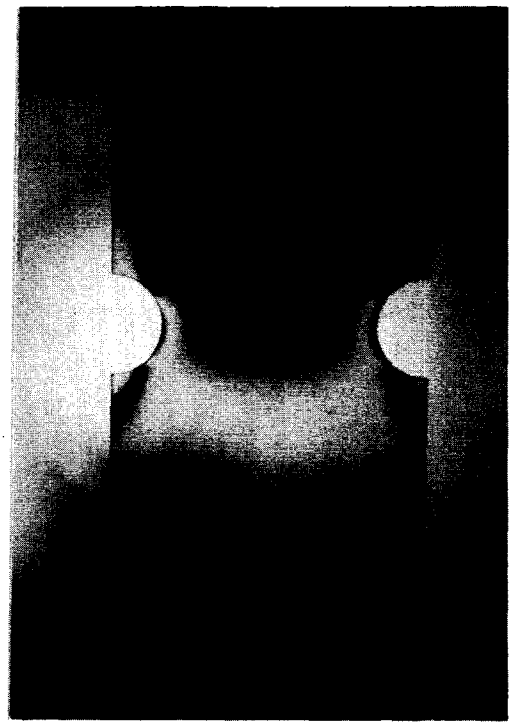

6. t = 1.9

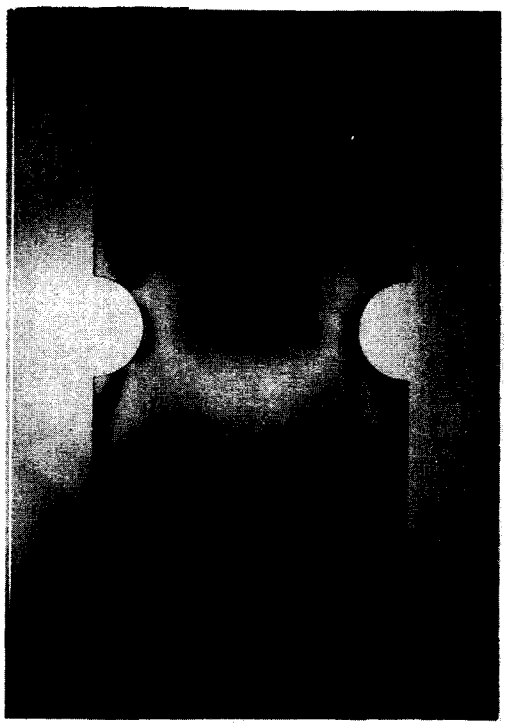

7. t = 2.0

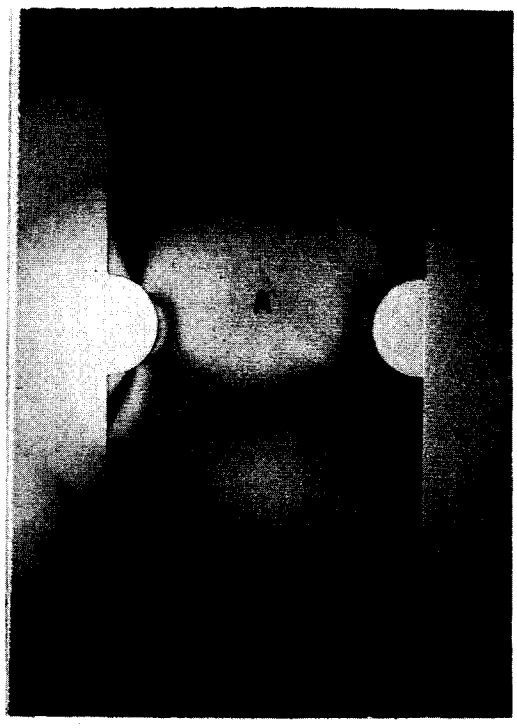

8. t = 2.1

Figure 6 (continued)

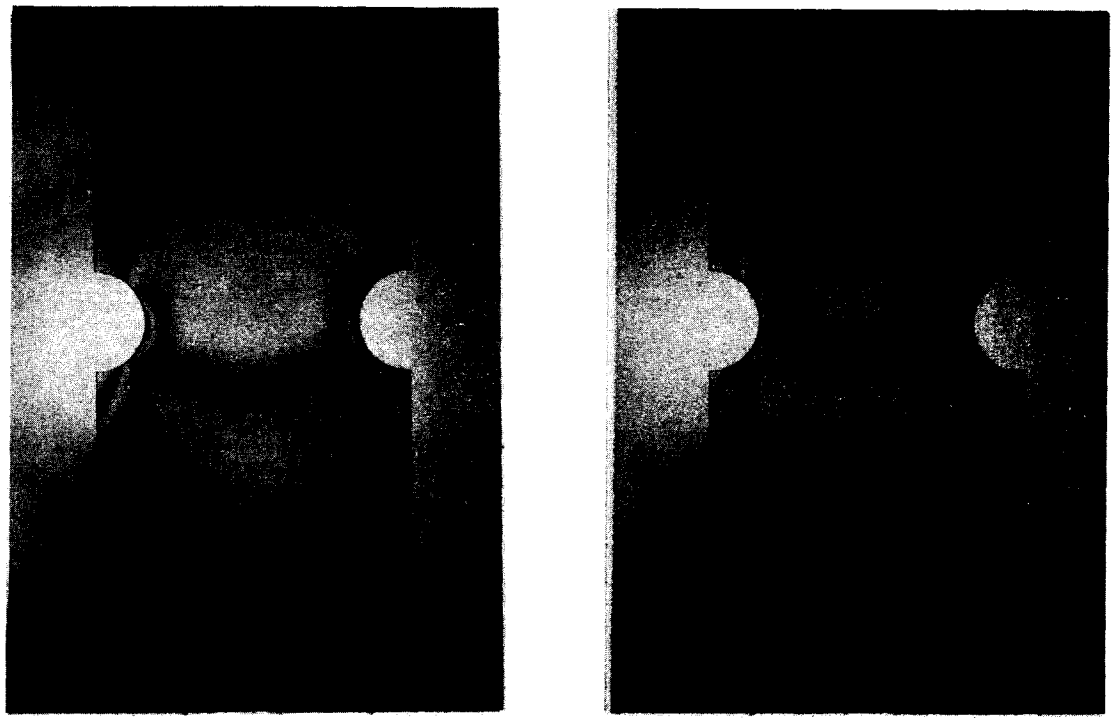

9· t = 2·2

10· t = 2·3

Figure 6 (continued)

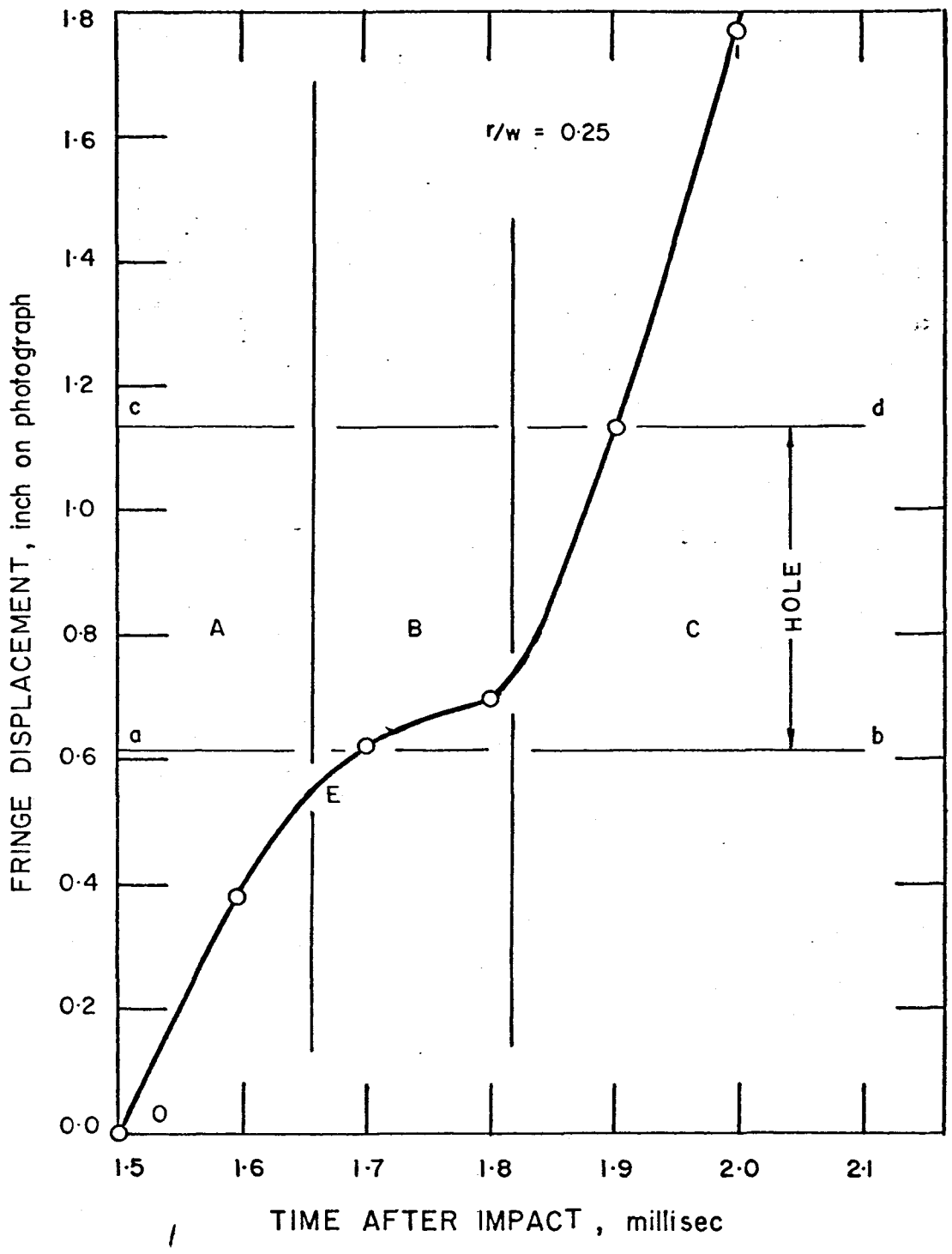

Figure 7 - Displacement of half-order fringe vs. time after impact

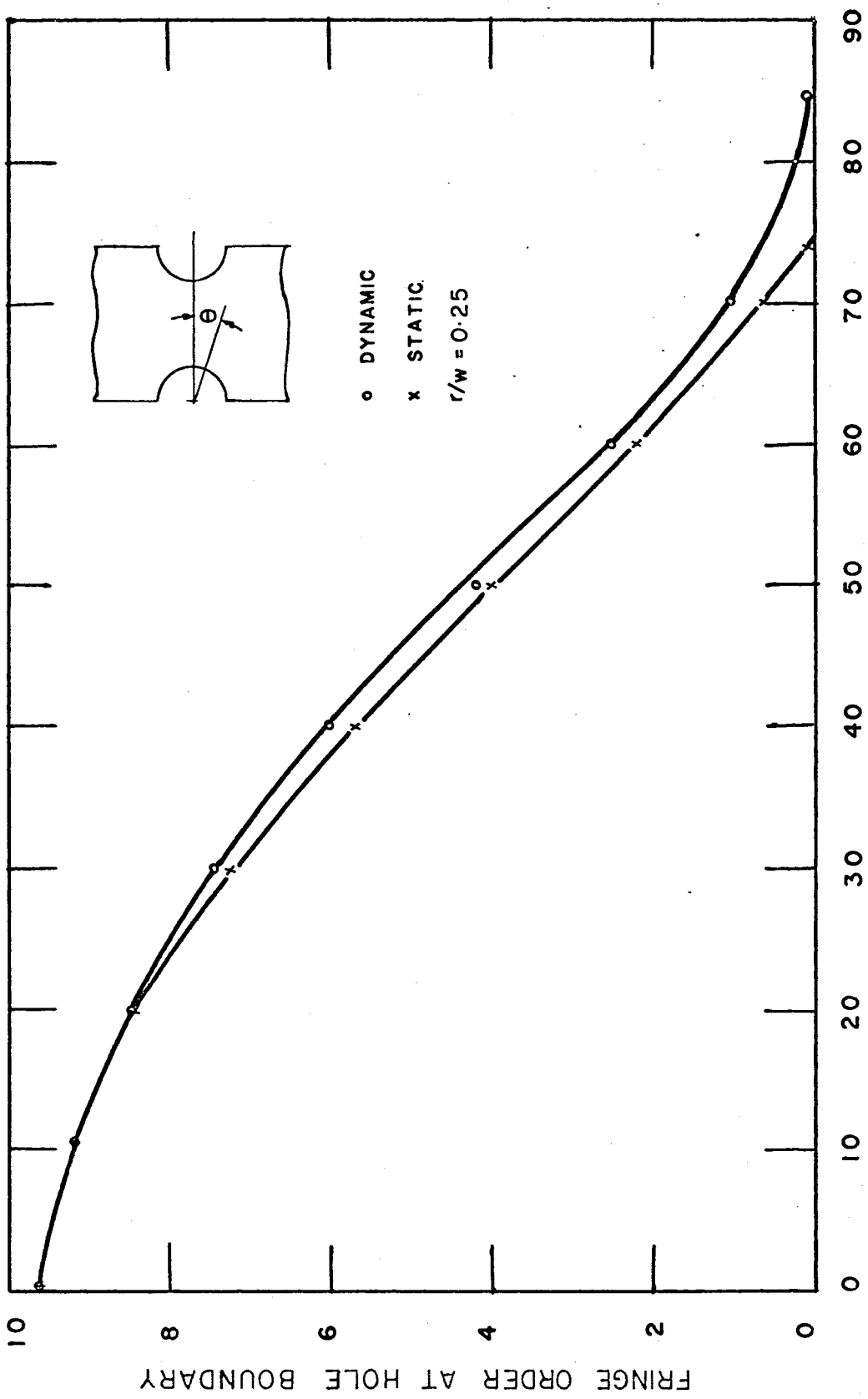

Figure 8 – Dynamic and static stress distribution around the discontinuity

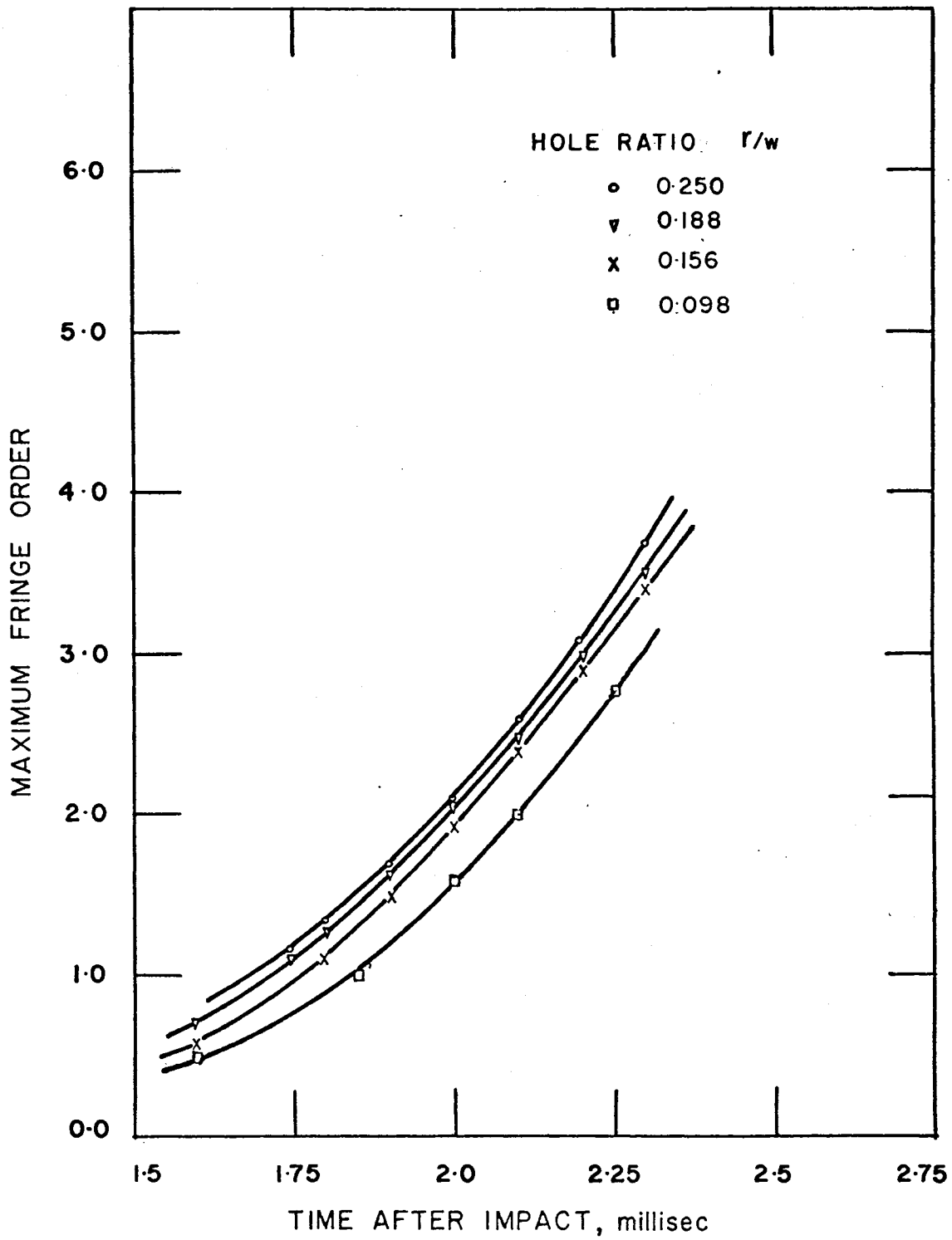

Figure 9 - Maximum fringe order at the discontinuity vs. time after impact

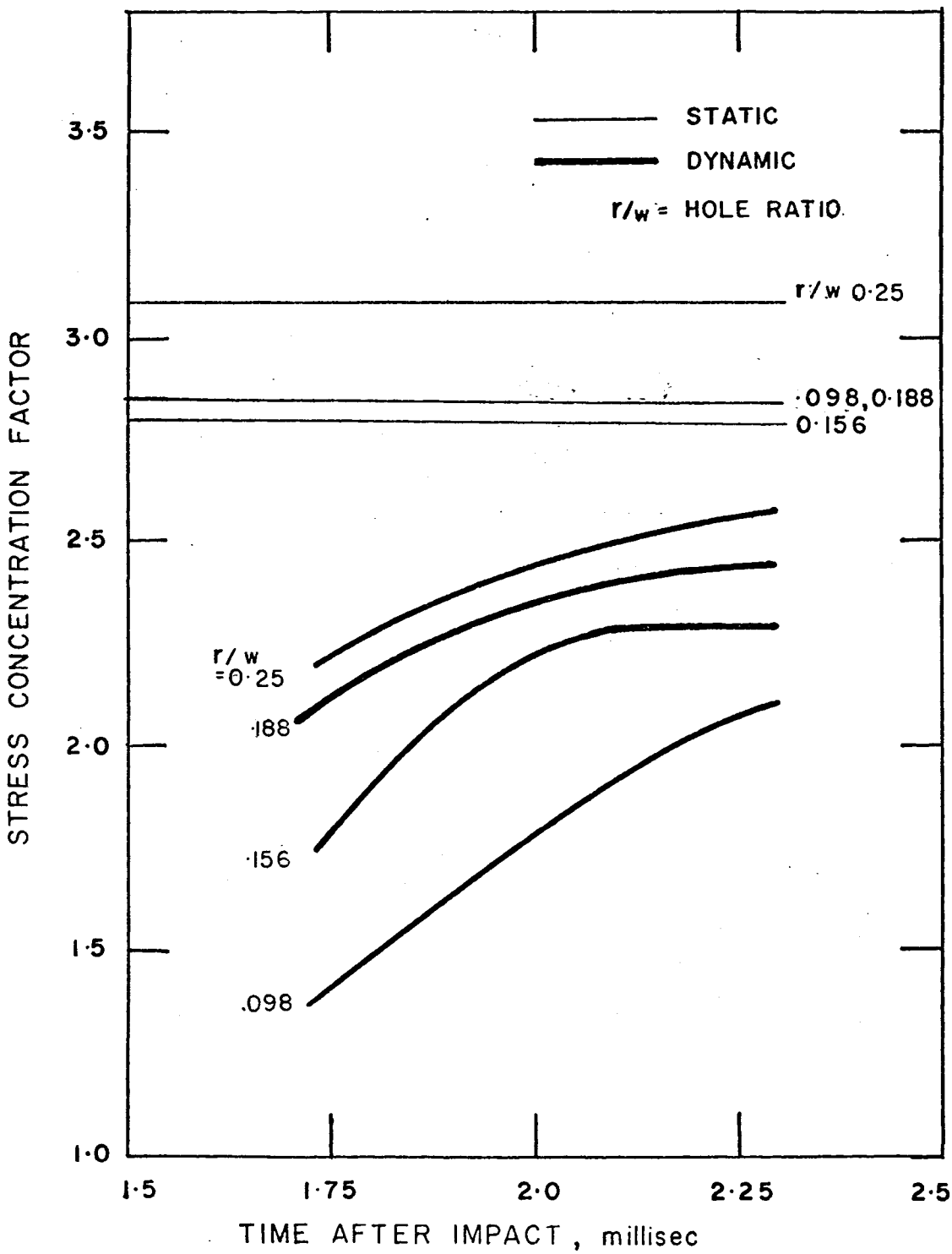

Figure 10 - Stress concentration factor vs. time after impact

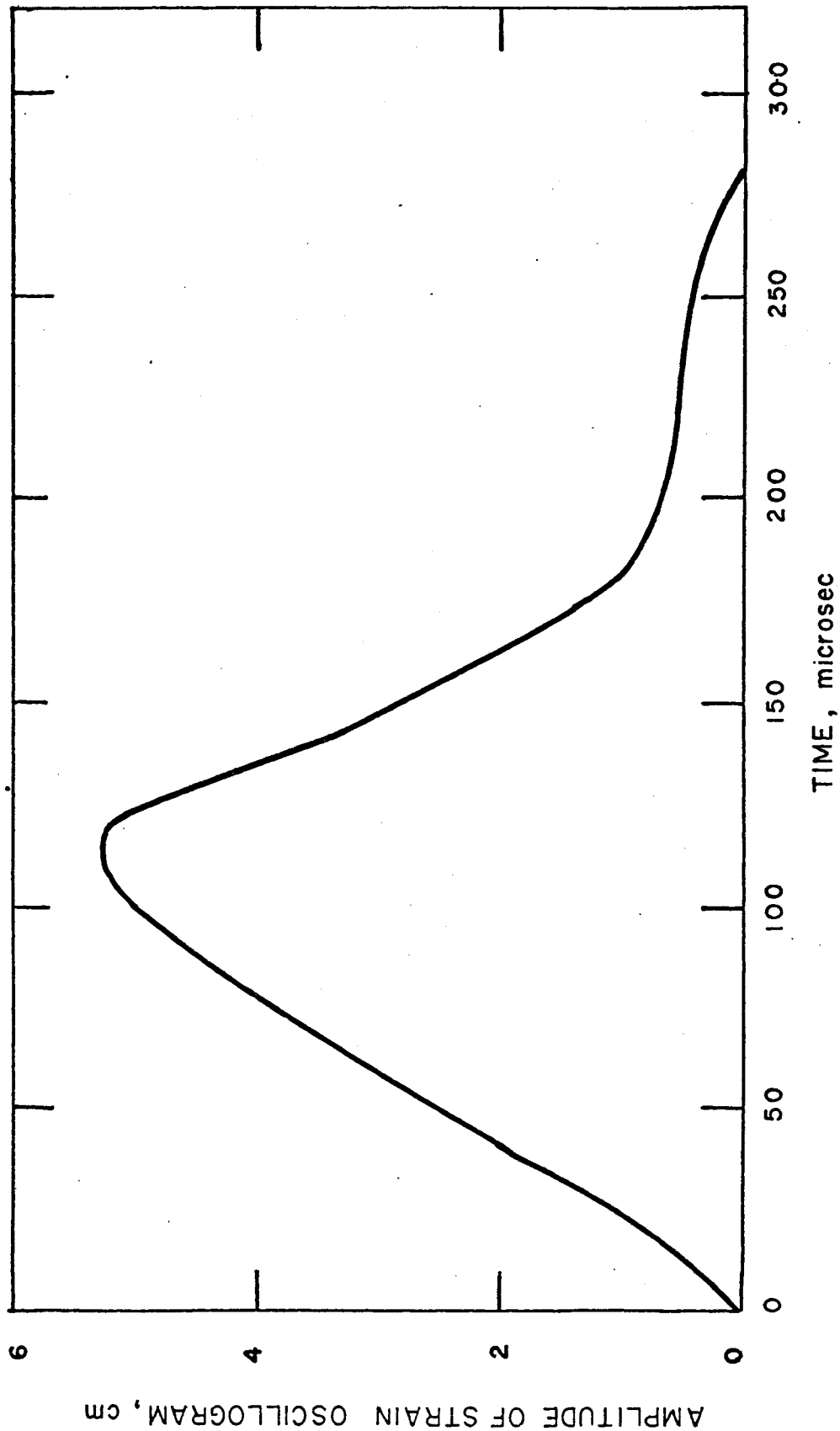

Figure 11 - Strain curve from the oscilloscope records (courtesy Ref. 1)

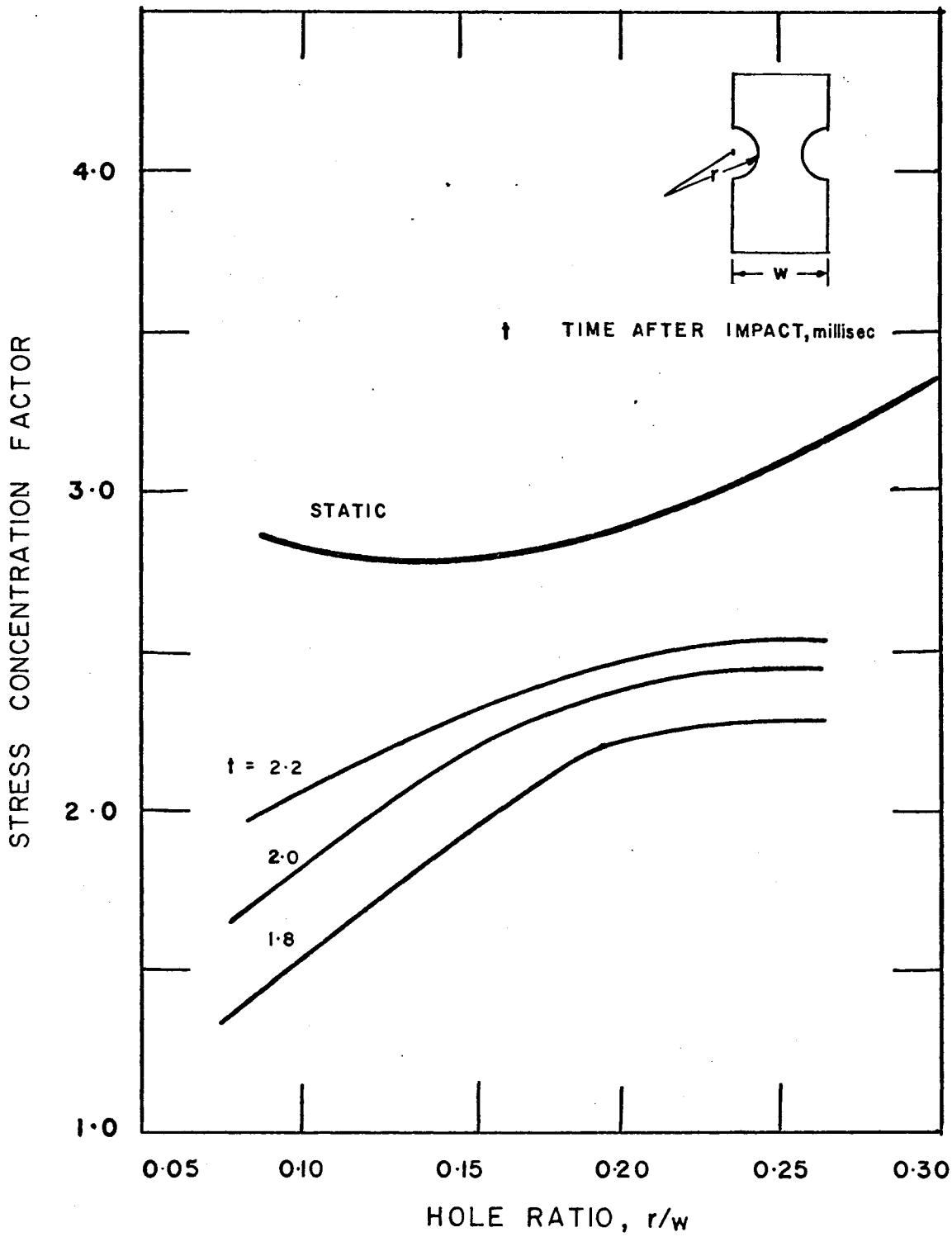

Figure 12 - Stress concentration factor vs. relative size of discontinuity

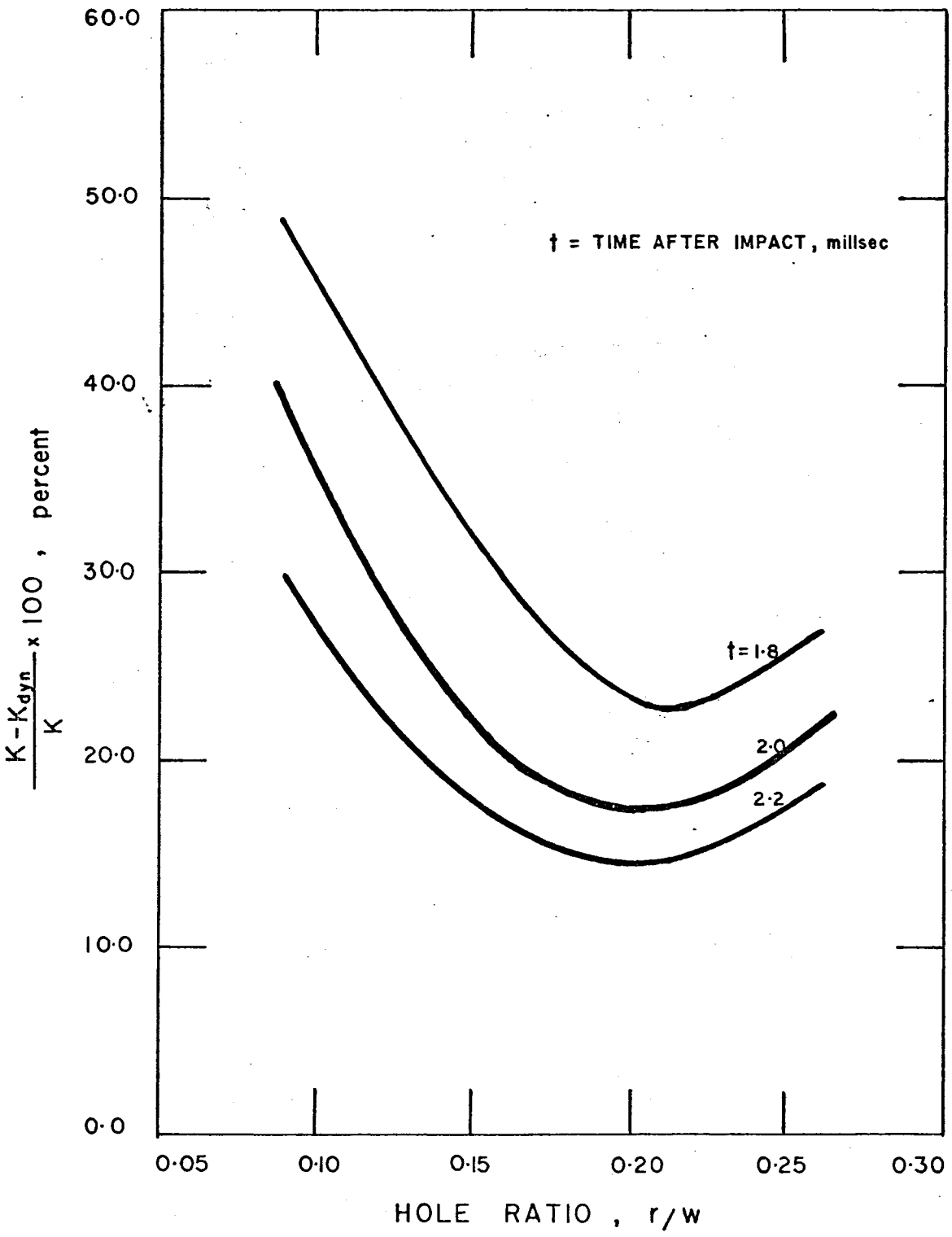

Figure 13 - Difference in dynamic and static concentration factor vs. time after impact

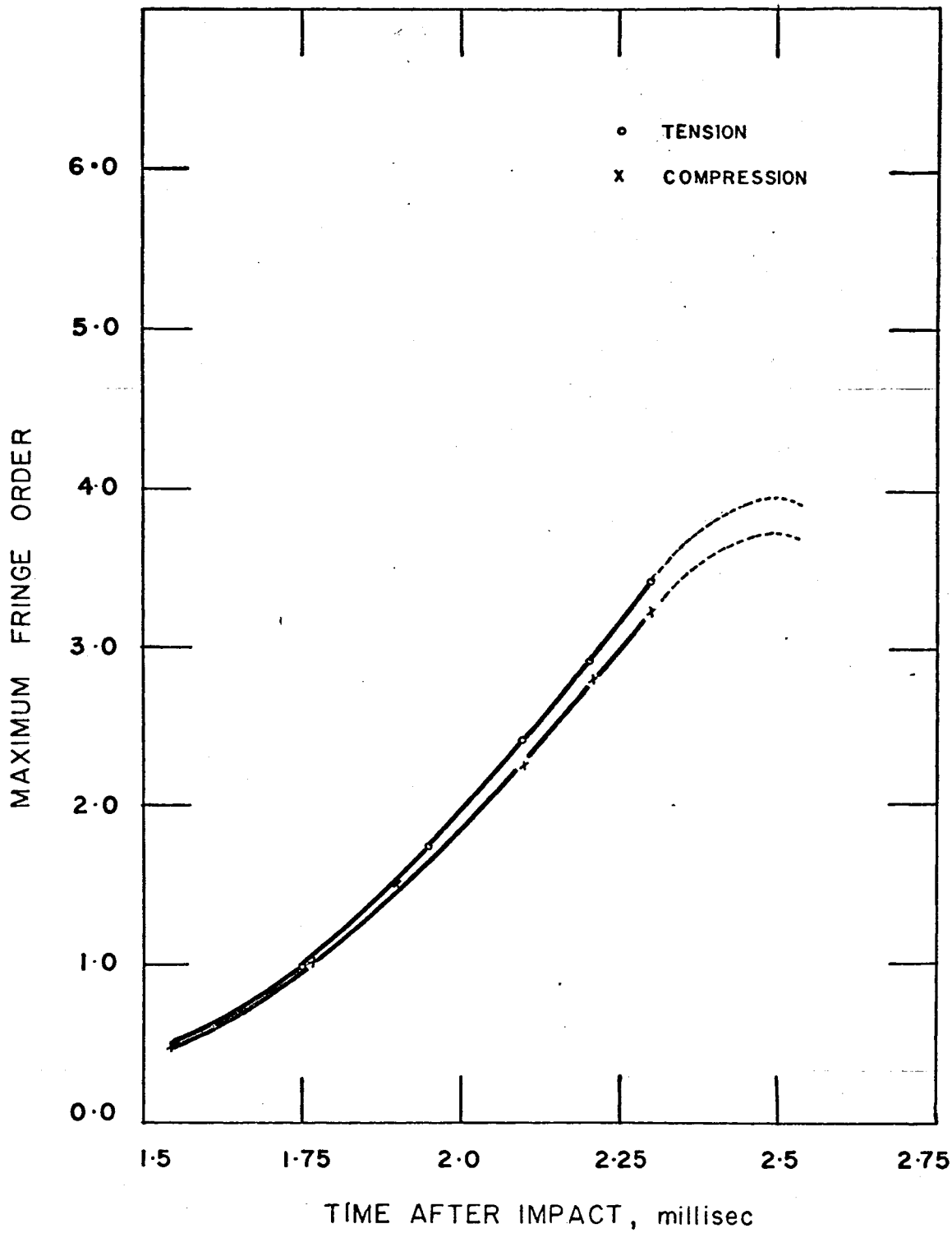

Figure 14 - Fringe order at the position of the discontinuity vs. time after impact in tension and compression in a model without discontinuity

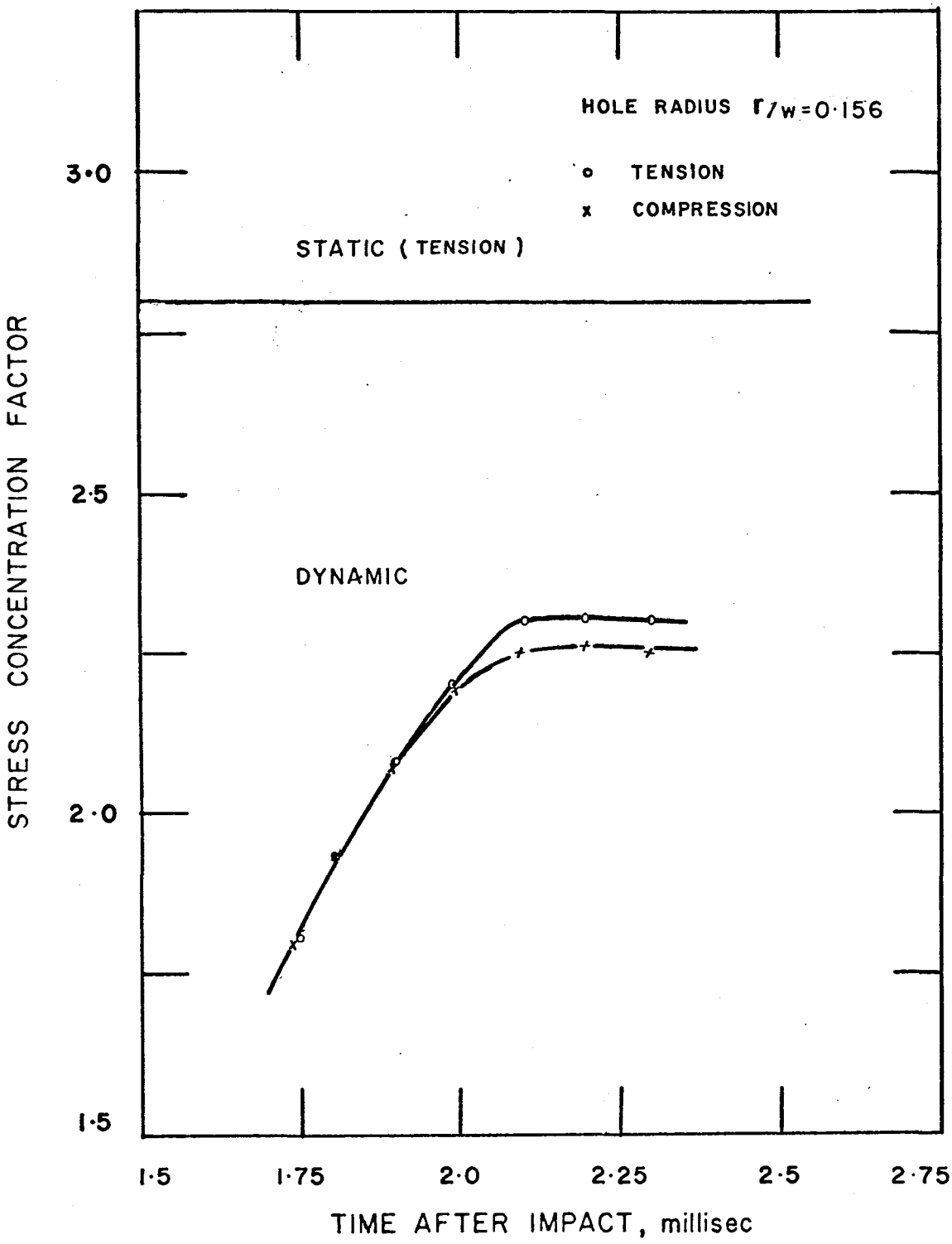

Figure 15 - Stress concentration factor vs. time after impact in tension and compression

APPENDIX A

CALIBRATION OF HYSOL 4485

A.1 Static Calibration

(1) Modulus of Elasticity - E

A specimen, fabricated from Hysol 4485 was loaded in tension. Figure A-1 shows the stress-strain curve obtained by measuring load and elongation.

The stress level attained during the experiment can be approximated to be in the range of 30 to 40 psi. The static stress-strain curve of figure 14 has an almost constant slope of 500 psi in this range. This gives E = 500 psi.

(2) Material Fringe Constant - f_σ

A circular disk of Hysol 4485 under diametral loading was tested for determining the material fringe constant. It was found that f_σ = 0.51 psi-in/fringe (based on shear stress).

(3) Density - ρ

Density of the material was found to be

$$= 0.000100 \ \frac{\text{lb-sec}^2}{\text{in}^4}$$

(4) Poisson's ratio is approximately 0.47.

A.2 Dynamic Calibration

A specimen of Hysol 4485 having the same dimensions as given in figure 3 but without a discontinuity was tested. Loading was in the same manner as in the case of models with discontinuities. Velocities of fringe propagation were obtained from the birefringent photographs of the test mentioned above. Figure A-2 shows the relation between velocity of propagation and the fringe order. Each fringe itself propagates with constant velocity, however.

Although no specific measurements were made for the dynamic calibration of Hysol 4485, the following can be estimated.

(1) Dynamic Modulus of Elasticity - E_d

The curve of figure A-2 was extrapolated to give the velocity of propagation of the zero order fringe as 3300 inch/sec. An approximation to the dynamic modulus of elasticity can be made by the relation $E_d = \rho c^2$, where

ρ is the mass density of material (0.000100 lb-sec^2/in^4) and c is the velocity of the zero order fringe (3300 in/sec) which gives

$$E_d = 1089 \text{ psi}$$

It should be noted that the accuracy of the above estimation would depend upon:

(i) The validity of assumptions that Poisson's ratio is zero, the material is elastic, no inertial

dispersion occurs, and that the waves are longitudinal; and

(ii) The accuracy in the determination of the velocity c.

(2) Dynamic Material Fringe Value

Previous authors have estimated the dynamic fringe value of Hysol 4485 to be about 9 per cent higher than the corresponding static value. Expecting similar behaviour of this material, the dynamic fringe value can be approximated to be 0.556 psi-in/fringe.

An attempt was made to determine the value of f_σ experimentally by the grid method [see Durelli and Riley (7)]. The analysis, however, could not be completed because of the lack of precise measurements of grid deformations. The procedure planned for its evaluation is outlined below for reference.

a. A model of the dimensions shown in figure 3, but without any discontinuity, is machined from a sheet of Hysol 4485, and a 1/8 in. square grid is scribed on its surface.

b. A no load photograph of the model is taken to record the undeformed grid pattern.

c. It is then loaded dynamically and the photographs of the fringe propagation are obtained in the manner outlined in section 4.3 of chapter four.

d. The displacement fields are obtained by measuring the deformation of the grid under loaded conditions from the photograph.

e. The strain fields are computed by differentiating the displacement fields.

f. Then the material strain fringe value is given by

$$f_\epsilon = \frac{\epsilon_y - \epsilon_x}{2N} \, h \qquad \text{(A.1)}$$

where ϵ_x and ϵ_y = axial and transverse strains respectively, at a point in the model computed from the displacement field, in/in.

N = Fringe order at the point

h = Model thickness, in

Then the stress fringe value

$$f_\sigma = \frac{E_d}{1+\nu} \cdot f_\epsilon \qquad \text{(A.2)}$$

where E_d = dynamic modulus of elasticity, psi

ν = dynamic Poisson's ratio

Dynamic Poisson's ratio can also be computed accurately from the information obtained in this experiment.

$$\text{Dynamic Poisson's ratio} = -\frac{\epsilon_y}{\epsilon_x} \qquad \text{(A.3)}$$

A.3 Stress Pulse Duration

It is estimated that the duration of stress pulse was not more than 1.25 milliseconds.

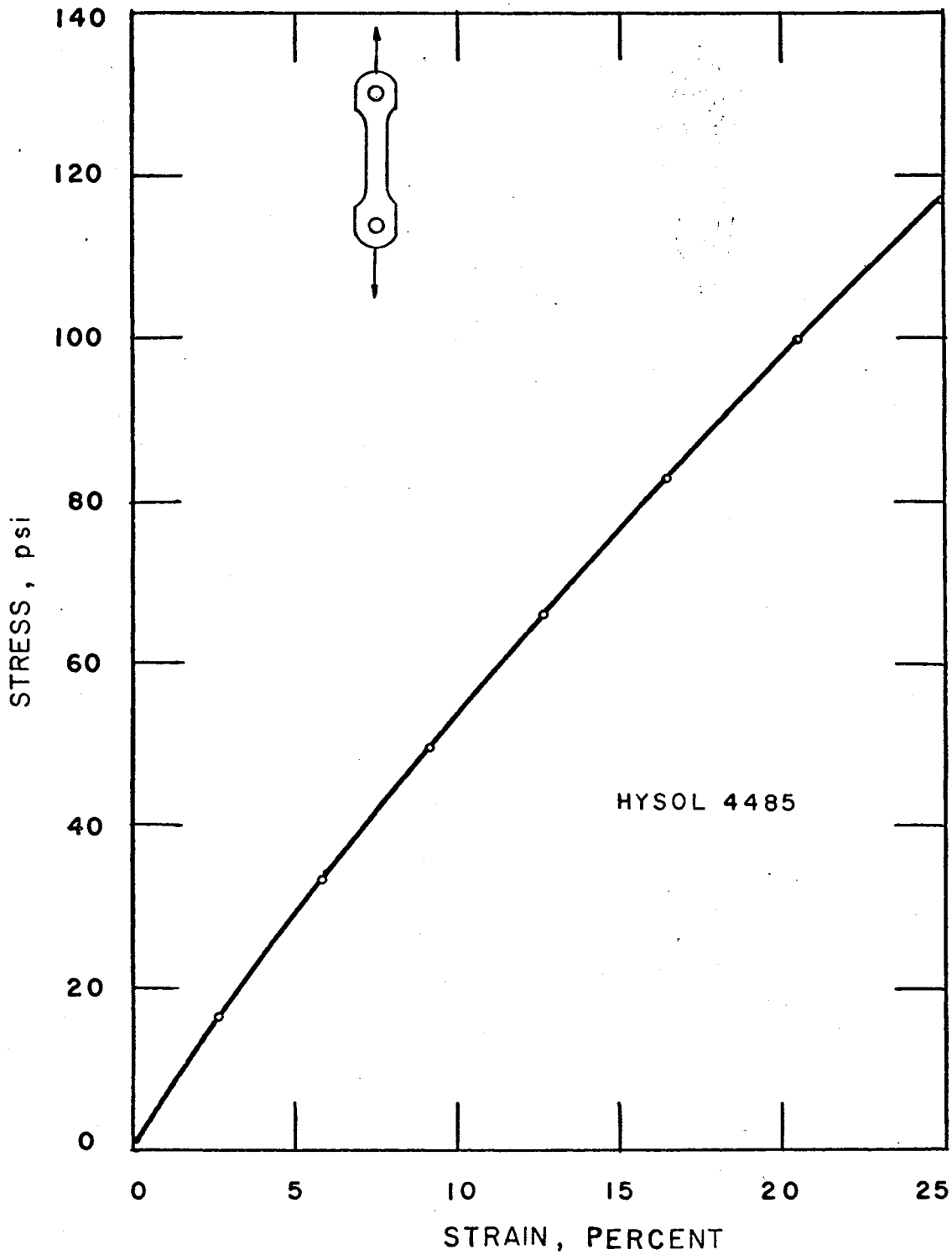

Figure A-1 - Static stress-strain curve

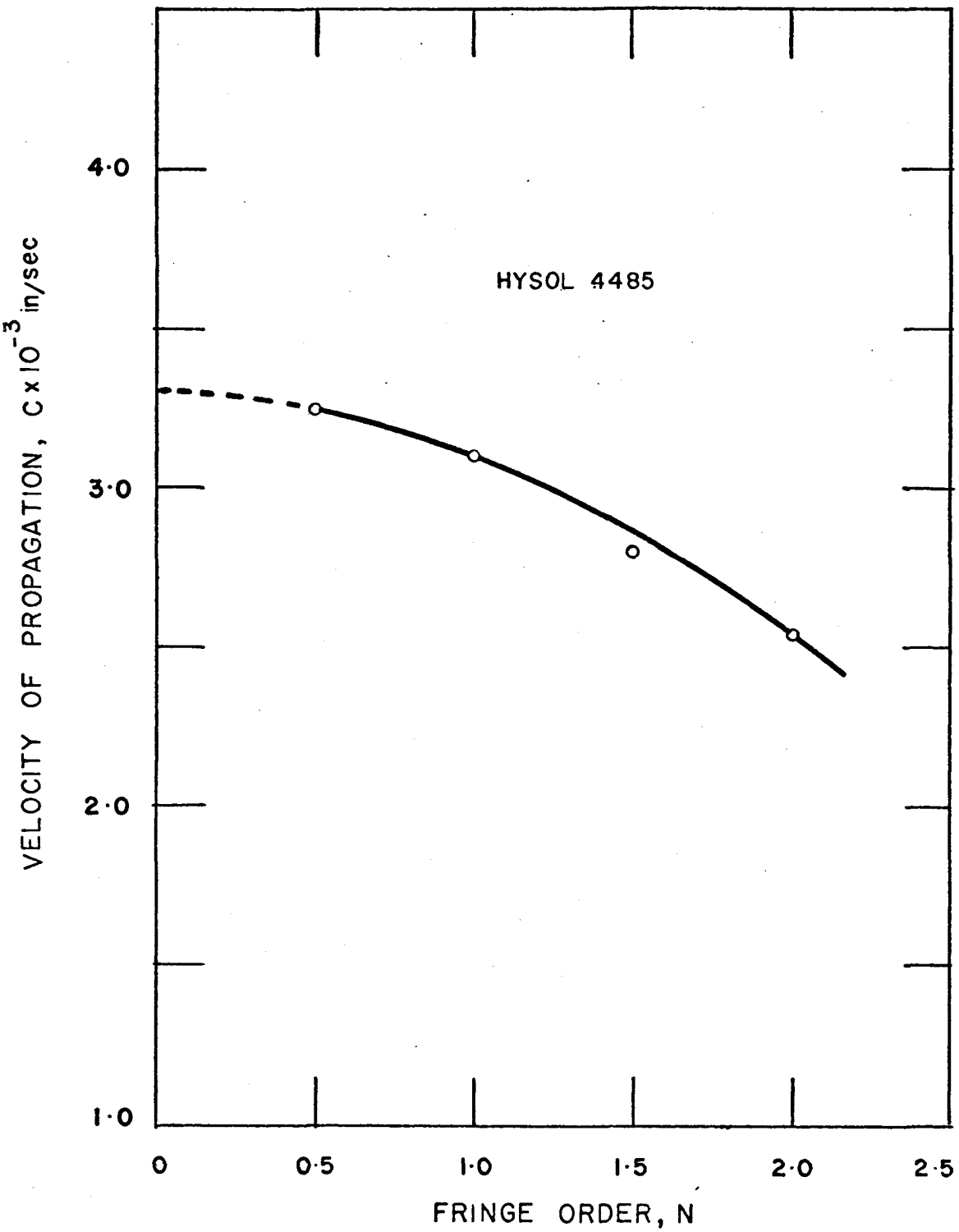

Figure A-2 - Velocity of propagation of different fringe orders

APPENDIX B

THEORETICAL AND EXPERIMENTAL DETERMINATION OF MAXIMUM STRESS DURING IMPACT

Theoretical estimation of the maximum stress in a bar in impact is based on the assumption that all of the potential energy of the falling mass is absorbed elastically in the bar in the form of the strain energy.

Let us consider a bar fixed at its upper end. A weight falls from the height h on to the flange ab, stretching the bar by an amount Δ . (See figure B-1.)

Then, the potential energy of the falling mass

$$= W(h + \Delta)$$

$$\simeq Wh \quad (\Delta \ll h) \qquad \text{(B.1)}$$

Elastic energy stored in the bar = $1/2\ P\Delta$

If P = static load to produce a deflection Δ in the bar

A = area of X-section of the bar

E = modulus of elasticity of the bar material

then $\Delta = P\ell/AE$

and the elastic energy = $P^2\ell/2AE$ (B.2)

From the basic assumption

Potential energy = elastic energy stored

or $Wh = P^2\ell/2AE$

or $Wh = \sigma^2 A\ell/2E$

i.e $\sigma = \sqrt{\frac{2\ Wh\ E}{A\ell}}$ (B.3)

where σ = induced stress

B.1 Stress in a Model Without Discontinuity

(1) Theoretical - The experimental values of different elements in equation (B.3) are as follows

$W = 1.5$ oz.

$h = 40$ inch

$E = 500$ psi

$A = 2 \times 0.25$ sq.in.

$\ell = 10$ inch

Then the theoretical stress in the bar from equation (B.3)

$\sigma_{theo} = 27.4$ psi (B.4)

(2) Experimental -

Maximum fringe order $N \simeq 4$ (figure 14)

Material fringe constant $f_\sigma = 0.556$ psi-in/fringe (Appendix A)

Then the experimental stress in the bar

$$\sigma_{exp} = 2\ N\ f_{\sigma}\ /h$$

$$= 17.8 \text{ psi} \qquad (B.5)$$

A comparison of (B.4) and (B.5) shows that the theoretical stress is about 54 per cent higher than the actual observed stress in the bar. It appears that this conservative prediction by theory is because of the incorrect basic assumption that all the potential energy of the falling mass is absorbed by the bar. In practice, however, a part of the energy would be lost during impact, thus reducing the effective stress.

B.2 Stress in a Model with Discontinuity

(1) Theoretical - If the static stress concentration factor is taken as representative, then the theoretical stress at the discontinuity

$$\sigma_{theo} = K \times 27.4 \text{ psi} \qquad (B.6)$$

And the experimental value of the stress at the discontinuity

$$\sigma_{exp} = K_{dyn} \times 17.8 \text{ psi} \qquad (B.7)$$

If the value of dynamic stress concentration factor be taken as 15 per cent lower than the corresponding static stress concentration factor, then

$$\sigma_{exp} = 0.85\ K \times 17.8 \text{ psi} \qquad (B.8)$$

A comparison of equations (B.6) and (B.8) indicates that the theoretical estimation of the stress at the discontinuity would be at least 80 per cent higher than the actual maximum stress developed in impact.

In this theoretical treatment, it must be assumed that a quasi-static state of stress is developed since the propagation of a stress wave is not conceded.

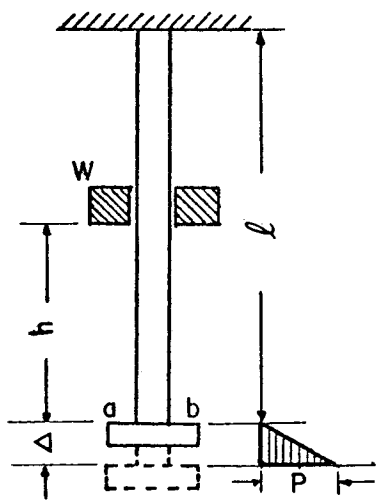

Figure B-1 - A bar subjected to impact

APPENDIX C

STRESS WAVE PROPAGATION IN A RECTANGULAR BAR

It has been mentioned that the effect of impact is propagated through the body in the form of elastic waves. In this study, the problem has been considered as that of the propagation of a longitudinal wave in an elastic bar. Following are the assumptions made:

(1) Cross-sections of the bar remain plane during deformation.

(2) Lateral motion of particles is unrestricted.

(3) Length of the wave is large compared to the cross-sectional dimensions of the bar.

Let us consider a bar subjected to an axial tensile impact. Strain in any section in x direction can be given by

$$\epsilon_x = \frac{\partial u}{\partial x} \qquad \text{(C.1)}$$

and the corresponding tensile force would be $AE \frac{\partial u}{\partial x}$,

where u = displacement in x direction

A = cross-sectional area

E = modulus of elasticity of the bar.

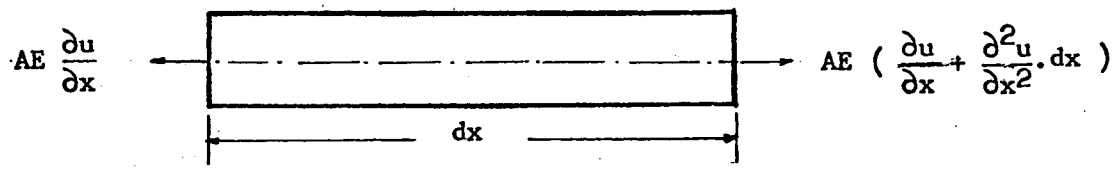

Figure C-1 - Free body diagram showing the forces on the two adjacent cross-sections of a bar subjected to axial tensile impact

Considering the free body diagram, the difference of forces acting on two adjacent cross-sections, dx apart, is

$$AE \left(\frac{\partial u}{\partial x} + \frac{\partial^2 u}{\partial x^2} \, dx\right) - AE \, \frac{\partial u}{\partial x}$$

$$= AE \, \frac{\partial^2 u}{\partial x^2} \, dx \qquad (C.2)$$

Deformation in x direction is a function of time as well. Hence, from Newton's Law

$$A \rho \, dx \, \frac{\partial^2 u}{\partial t^2} = AE \, \frac{\partial^2 u}{\partial x^2} \, dx$$

where ρ is the density of the bar. So that

$$\frac{\partial^2 u}{\partial t^2} = \frac{E}{\rho} \, \frac{\partial^2 u}{\partial x^2}$$

or
$$\frac{\partial^2 u}{\partial t^2} = c^2 \, \frac{\partial^2 u}{\partial x^2} \qquad (C.3)$$

where c
$$= \sqrt{\frac{E}{\rho}} \qquad (C.4)$$

The general solution of equation (C.3) is

$$u = f(x+ct) + G(x-ct) \qquad (C.5)$$

From the simple physical considerations, it can be shown that the second part of equation (C.5) represents a wave travelling in the direction of x-axis with a constant speed c;

and the first part represents a wave travelling in opposite direction with the same velocity. It should be noted that the velocity of propagation depends only on the material properties E and ρ.

The arbitrariness of solution (C.5) can be removed with the help of initial conditions of the problem concerned.

C.1 Fixed Bar Subjected to Impact

Let us consider the case of a bar of uniform cross-section loaded at one end by a suddenly applied uniform tensile stress σ (see figure C-2). It will develop a tensile zone of very thin layers, particles of which would move with a velocity V.

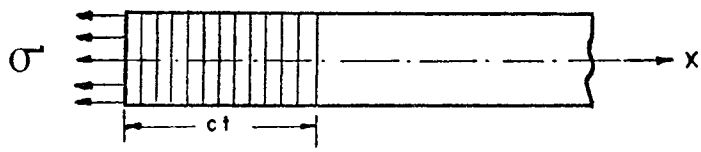

Figure C-2 - Expansion zone in a prismatic bar subjected to impact

If we take the direction of the wave propagation as positive direction, the change in the length ct of the expanded zone = $\frac{-\sigma}{E}$ ct; and therefore, the velocity of the particles in this region is

$$V = -\frac{\sigma}{E} c t/t$$

$$= -\frac{\sigma}{E} c \qquad (C.6)$$

Substituting the value of c from equation (C.4),

$$V = -\frac{\sigma}{\sqrt{E\rho}} \qquad (C.7)$$

Minus sign indicates that the velocity of the particles in the expansion zone is in a direction opposite to the direction of wave propagation.

Let a rigid body with an impact velocity V_o hit the free end of the bar, producing a uniform initial tensile stress σ_o. From equation (C.7), this initial stress would be

$$\sigma_o = -V_o\sqrt{E\rho} \qquad (C.8)$$

By Newton's Law, the impact force in the expansion zone is balanced as given by the following relation

$$m \frac{dv}{dt} = -(-\sigma A)$$

or $$M \frac{dv}{dt} - \sigma = 0 \qquad (C.9)$$

where $$M = \frac{m}{A}$$

$$= \frac{\text{mass of the moving body}}{\text{Area of cross-section of the bar}}$$

Substituting the value of $\frac{dv}{dt}$ in equation (C.9) from equation (C.7), we have

$$\frac{M}{\sqrt{E\rho}} \cdot \frac{d\sigma}{dt} + \sigma = 0 \qquad (C.10)$$

Solution of this differential equation is

$$\sigma = \sigma_o \exp\left(-\frac{\sqrt{E\rho}}{M} t\right) \qquad (C.11)$$

Equation (C.11), therefore, gives the stress at the end of the bar at any time t after impact.

C.2 Effect of Variable Cross-Section

If the area of cross-section of the bar is not uniform, i.e. A = A(x), then the equation (C.10) becomes

$$\frac{m}{\sqrt{E\rho}} \cdot \frac{1}{A(x)} \frac{d\sigma}{dt} + \sigma = 0$$

The above equation involves two independent variables and therefore is not easily solved as such. This indicates that a case involving a bar with a discontinuity cannot be solved by the theoretical considerations based on the elastic wave propagation.

An estimate of the maximum stress in a model without discontinuity can be made based on the assumption that the stress propagates without dispersion down the bar.

From equation (C.8), the maximum stress that occurs at the end of the bar

$$\sigma_o = - V_o\sqrt{E\rho}$$

where V_o = velocity of impact

= 176.0 in/sec (a weight falling through 40 in)

Then, $\sigma_o = - 176.0 \sqrt{.0001 \times 1089}$

= 58.0 psi (C.12)

If the static stress concentration factor is taken as representative, then the maximum stress in a model with discontinuity is

$$\sigma_o = 58.0 \times K \text{ psi} \qquad \text{(C.13)}$$

Again, if the value of dynamic stress concentration factor is taken as 15 per cent lower than the corresponding static stress concentration factor, then from equation (B.8)

$$\sigma_{exp} = 0.85\ K \times 17.8 \text{ psi} \qquad \text{(B.8)}$$

Hence, per cent difference in the theoretical and experimental estimation of maximum stress

$$= 280 \text{ per cent} \qquad \text{(C.14)}$$

APPENDIX D

DESCRIPTION OF EQUIPMENT

D.1 Main Equipment

Figure 1 is a block diagram showing the different components of the experimental setup used. The actual arrangement of the laboratory equipment is shown in the photograph of figure 2. Table 1 lists the essential components with their specifications.

Table 1 - Main components of the experimental equipment used

No.	COMPONENT	DETAILS
1	Light Source	Philips Stroboscope PR 9104 Flash duration 10μsec.
2	Polariscope	8-1/2 inch field circular polariscope
3	Camera	Graflex Camera with polaroid back and long extension bellows
4	Loading frame	With the provision of the adjustments in all the three planes to centre the falling mass on to the model
5	Loading cell	Used to produce tension. Fabricated from Bakelite

D.2 Circuit Diagrams

The following circuits were designed and assembled by Central Research Shop of the University of Windsor.

(1) Delay Circuit: A delay circuit having the provision of giving two identical outputs was designed for the electronic switching of a laser power supply. The circuit shown in figure D-1 provided the delay ranging from 1 millisecond to 9 milliseconds. It had shown a high repeatability to the extent of almost 100 per cent.

(2) Photo Trigger: One major problem involved in the experiment is to accomplish highly repetitive fast switching of the light source. Initially, the falling mass itself was used to provide the triggering pulse by activating the photo-cell circuit, shown in figure D-2. At a later stage, however, the photocell was used only to permit monitoring of the time delay after impact and the primary triggering was initiated by the falling mass which shorted an electrical contact. Figure D-3 shows an electromagnet arrangement made to drop the weight.

(3) Regulated Power Supply: A transistorized, regulated power supply was also assembled (figure D-4). This had the provision of supplying 21, 10, 5, and 2 volts needed for the various circuits shown in figures D-1 through D-3. This

circuit was an integrated part of the delay assembly of figure D-1.

(4) Light Output Recorder and its Power Supply: Figures D-5 and D-6 show the circuits of the light output recorder and its power supply respectively. The circuit was initially designed for recording the output of a ruby laser and had a very fast rise time of about 10 nanoseconds. A trace of the light pulse from the stroboscope, as obtained with the help of the recorder is shown in figure D-7.

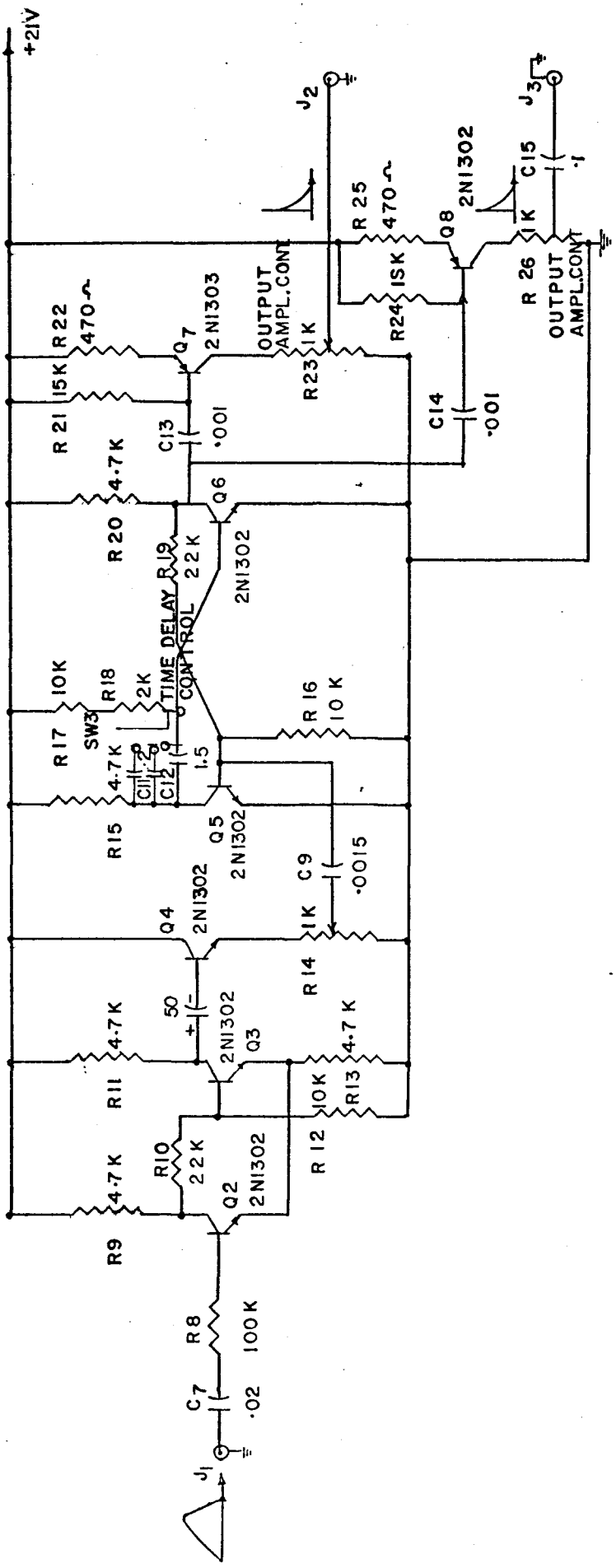

D-1 - Circuit diagram of transistorized time delay unit

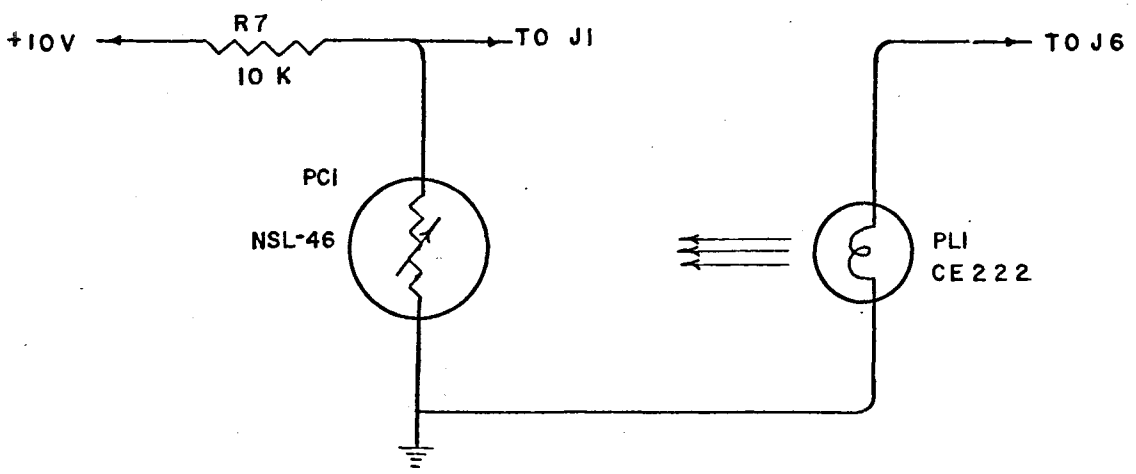

Figure D-2 - Photocell circuit

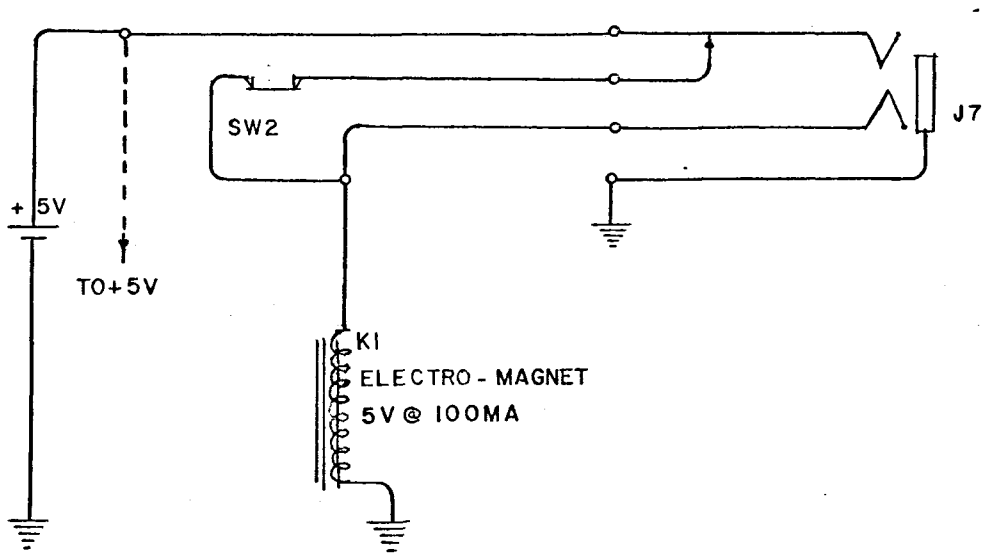

Figure D-3 - Electromagnet arrangement

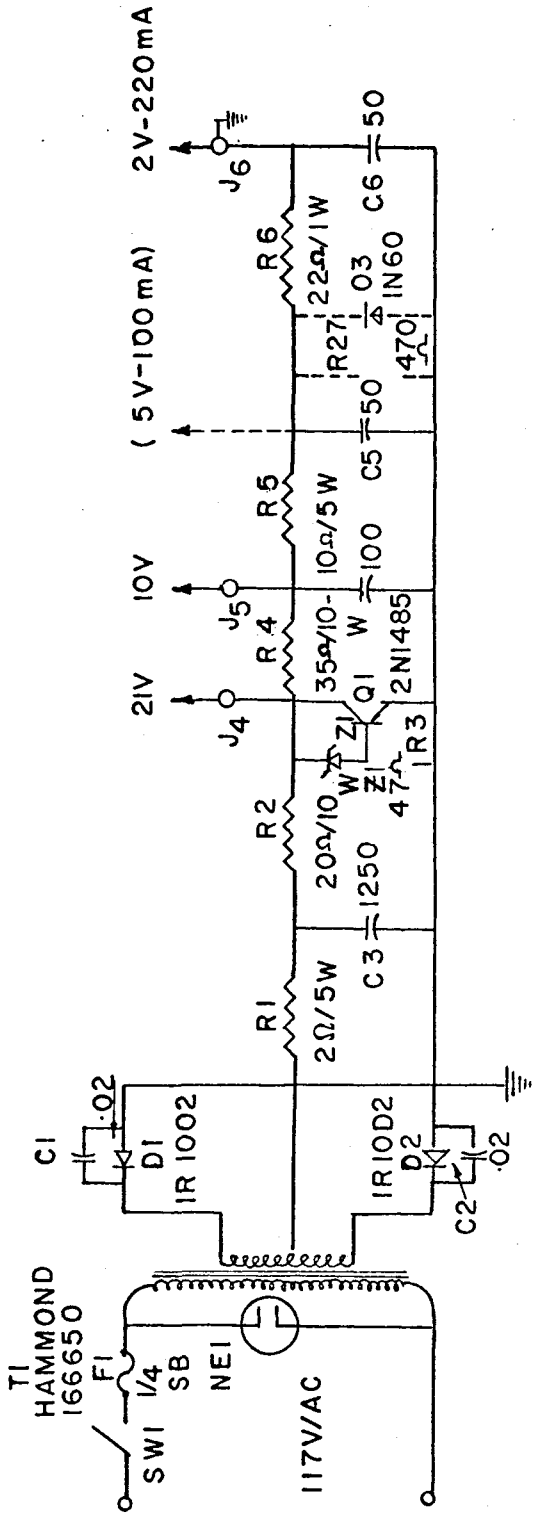

Figure D-4 - Regulated power supply for the circuits shown in Figures D-1 through D-3

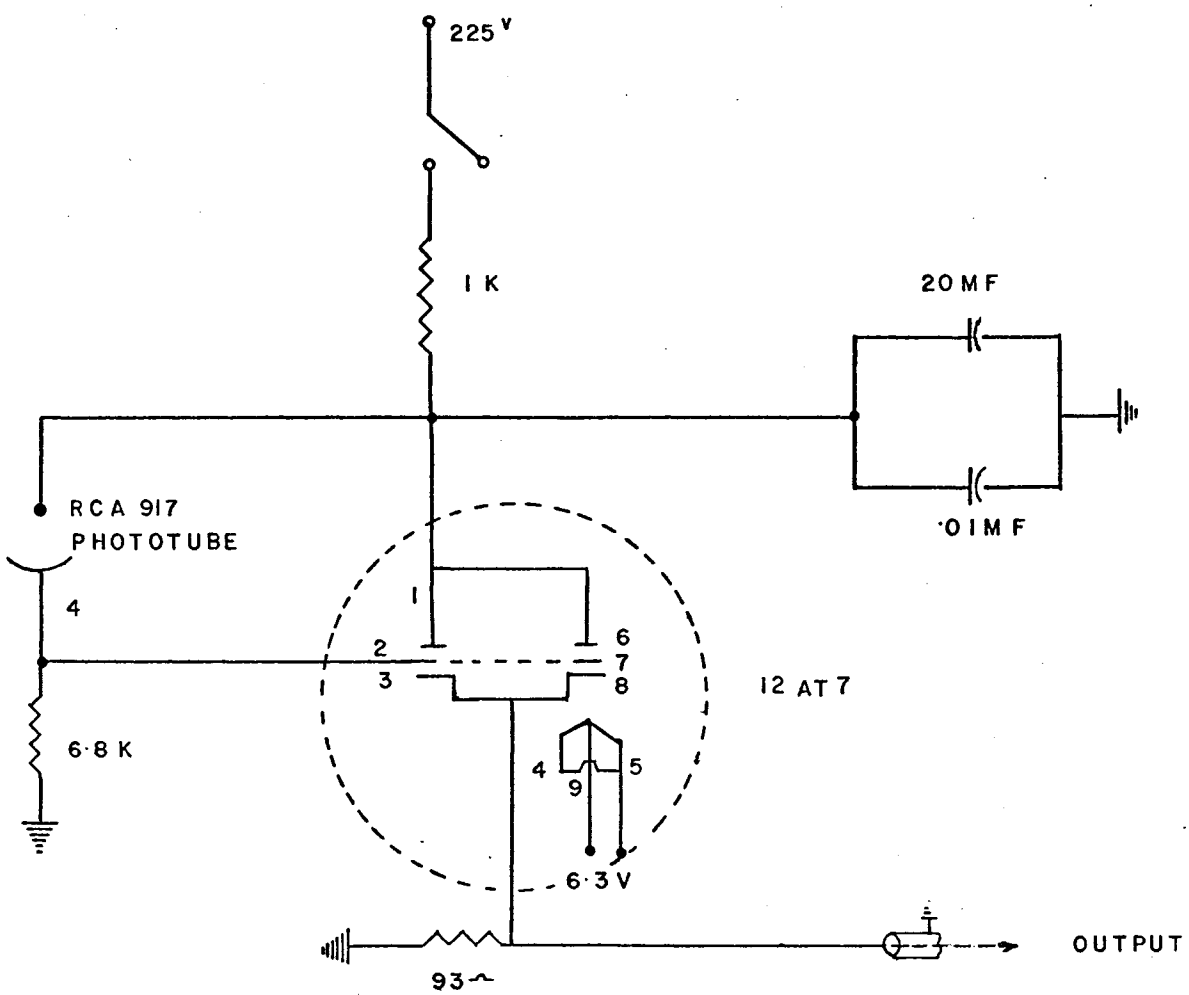

Figure D-5 - Circuit of the light output recorder

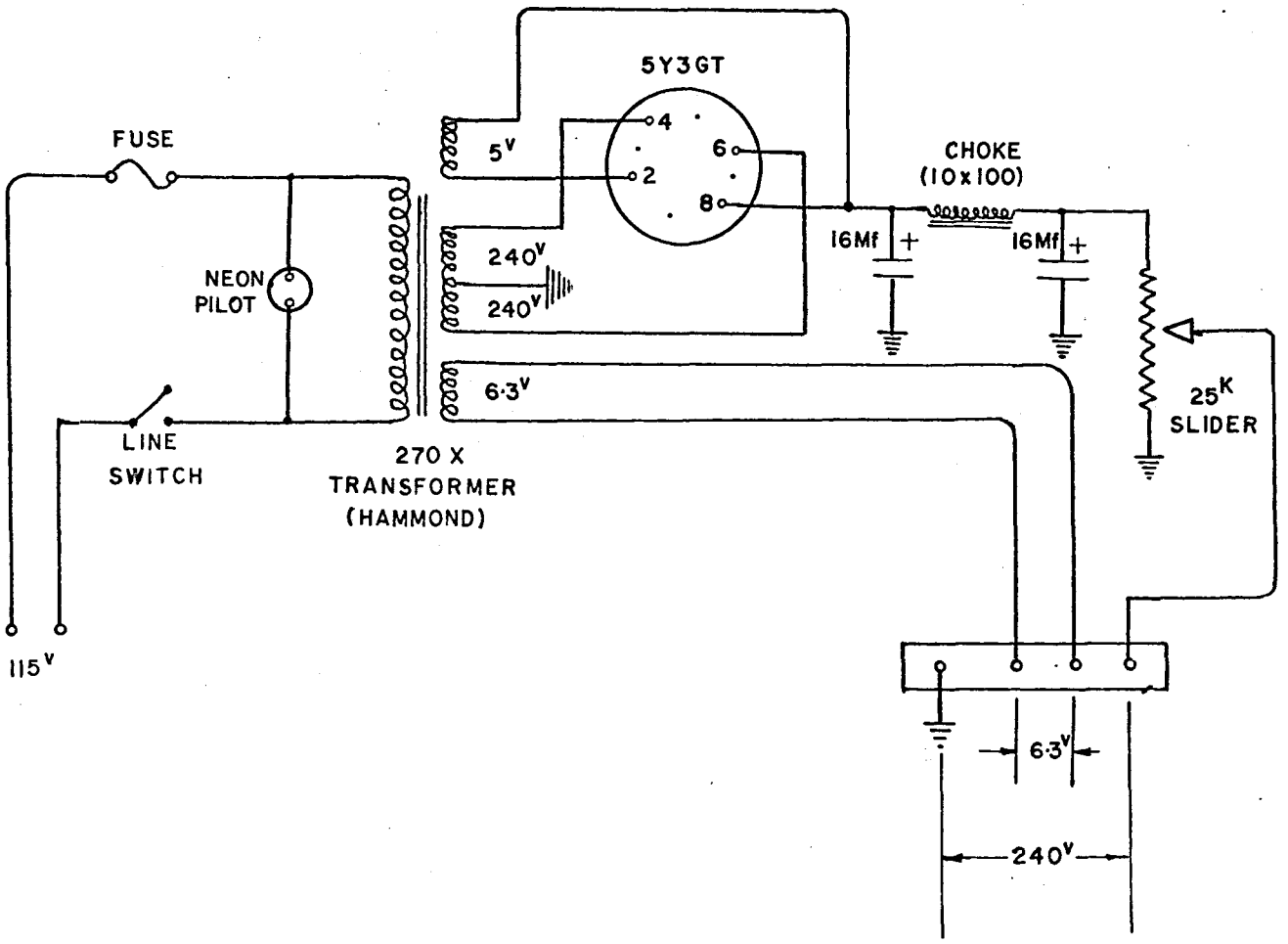

Figure D-6 - Power supply for the output recorder

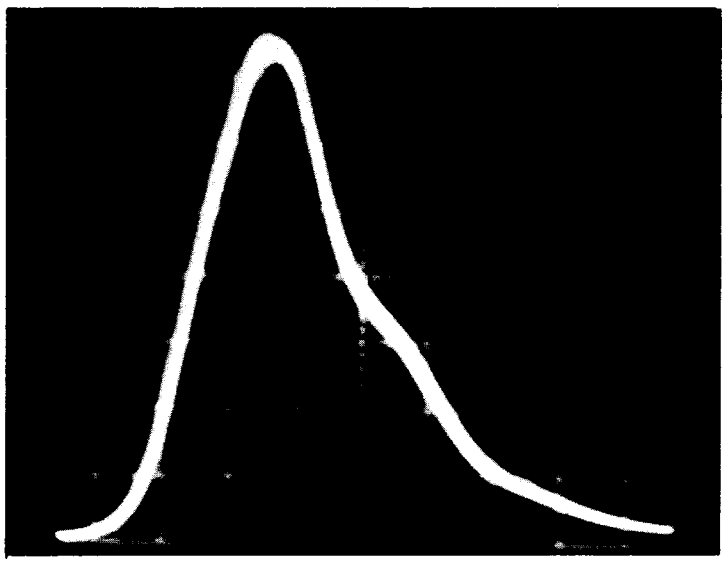

Figure D-7 - Light pulse from the stroboscope
Horizontal scale - 5 μsec/division
Vertical scale - 0.1 volt/division
Pulse duration - 10 μsec (as measured at 50% of the pulse height)

APPENDIX E

PHOTOELASTICITY - BASIS OF ITS THEORY AND RELATED INFORMATION

E.1 Optical Interference and Simple Polariscope

The necessary condition for the light waves to combine to yield optical interference is that they must be coherent and should be polarized in the same plane. A polariscope is a system that serves this purpose by transmitting only those components of the two interfering rays that lie in a common plane, so that the optical interference can ensue.

A plane polariscope consists of a light source, a polarizer and an analyzer, arranged in the order shown in figure E-1. A doubly refracting plate has also been inserted in between the polarizer and analyzer, with one of its axes making an angle θ with the axis of polarization.

Let the plane polarized light vector emerging from the polarizer be represented by the equation

$$A_{11} = a \sin(\omega t) \qquad \text{(E.1)}$$

where a = amplitude of the light vector

ω = angular frequency

t = time.

The vector A_{11} upon entering the doubly refracting plate is resolved into two components given by

$$A_{21} = a \cos\theta \cdot \sin(\omega t) \qquad (E.2)$$

$$A_{22} = a \sin\theta \cdot \sin(\omega t)$$

Let Δ be the relative retardation of the emerging vectors, which can be represented by

$$A_{31} = a \cos\theta \cdot \sin(\omega t)$$

$$A_{32} = a \sin\theta \cdot \sin(\omega t + \Delta) \qquad (E.3)$$

Then from figure E-1, the vector emerging from the analyzer is given by

$$\begin{aligned} A_{41} &= A_{32} \cos\theta - A_{31} \sin\theta \\ &= a \sin\theta \cos\theta \sin(\omega t + \Delta) - a \cos\theta \sin\theta \sin\omega t \\ &= [a \sin 2\theta \sin(\Delta/2)] \\ &\quad [\cos(\omega t) \cos(\Delta/2) - \sin(\omega t) \cdot \sin(\Delta/2)] \\ &= b \cos(\omega t + \Delta/2) \qquad (E.4) \end{aligned}$$

where $b = a \sin(2\theta) \sin(\Delta/2)$

$=$ the amplitude of the emerging light vectors

The intensity of the light as recorded is proportional to the square of the amplitude of the light vector emerging from the analyzer. Therefore, intensity

$$I = K \sin^2(2\theta) \sin^2(\Delta/2) \cos^2(\omega t + \Delta/2) \qquad (E.5)$$

Light extinction is obtained when $I = 0$, which can be achieved in the following three ways:

(a) When $(\omega t + \Delta/2) = [(2m + 1)\pi]/2$, (m = 0,1,2,etc.) (E.6)

In this case, however, the circular frequency ω is so high that this periodic extinction cannot be recorded and, therefore, this factor can be ignored.

(b) When $\theta = m\pi/2$, (m = 0, 1, 2, etc.) (E.7)

i.e. when one principal axis of the doubly refracting plate is parallel to the polarization plane.

(c) When $\Delta/2 = m\pi$, (m = 0, 1, 2, etc.)

or, $\Delta/2\pi = m$ (E.8)

i.e. when relative retardation is an integral number of cycles of retardation.

E.2 Photoelasticity

Photoelastic materials have a remarkable property of becoming double refracting when stressed. A ray of polarized light incident on such material is split into two components, each vibrating along a principal axis of the stressed body. The indices of refraction of these two light paths are proportional to the magnitude of the principal stresses.

These two emerging light waves, having suffered relative retardation because of the difference in the refraction indices of two paths, produce interference when brought together in a polariscope. The constructive and the destruc-

tive interference thus obtained develops a photoelastic pattern of dark and light bands, depending upon the degree of relative retardation of the two emerging waves. These light and dark bands are called isochromatic fringes. Obviously, therefore, this relative retardation or eventually the isochromatic fringe pattern is a function of the state of stress at each point in the body.

E.3 Stress Optic Law

The principal stresses induced in the model, and the resulting change in the refractive indices described above are related by the following relation

$$n = c\,(\sigma_1 - \sigma_2) \qquad \text{(E.9)}$$

where n = relative change in the refractive indices of two paths

c = relative stress optic coefficient

σ_1 , σ_2 = principal stresses

This difference n in the refraction indices can be related to the relative retardation of the emerging waves by

$$n = \Delta \cdot \frac{\lambda}{2\pi h} \qquad \text{(E.10)}$$

where Δ = relative phase shift produced by the model because of its double refractive behaviour

λ = wavelength of the light

h = model thickness

Equations (E.9) and (E.10) give the stress optic law as

$$\Delta = \frac{2\pi}{\lambda} h \cdot c \left(\sigma_1' - \sigma_2' \right) \qquad \text{(E.11)}$$

This can be rearranged as

$$\sigma_1' - \sigma_2' = \frac{\Delta}{2\pi} \cdot \frac{\lambda}{c} \cdot \frac{1}{t}$$

or $$\frac{\sigma_1' - \sigma_2'}{2} = N \cdot \frac{f_\sigma}{h} \qquad \text{(E.12)}$$

where $N = \frac{\Delta}{2\pi}$, the relative retardation of the emerging waves (dimensionless)

= isochromatic fringe order

f_σ = the material fringe value, psi-in/fringe (based on shear)

h = the model thickness, in

The material fringe value f_σ is determined experimentally.

Relation (E.12) indicates that the difference of the two principal stresses at any point in the body can be determined by counting the corresponding isochromatic fringe order, and that every band is the locus of the points of constant maximum shear stress.

E.4 Isoclinics

It has been shown that extinction is also obtained at points where one principal stress axis of the stressed model is parallel to the plane of polarization [equation (E.7)]. The locus of all such points is a dark band and is called an isoclinic.

An isoclinic is always superimposed on the isochromatic fringe pattern. If white light is being used, it can be distinguished from the zero order isochromatic fringe by rotating the system of polarizer and analyzer simultaneously in a plane polariscope. The isoclinic would move with the rotation of the system, whereas a fringe would not.

This new pattern of isoclinics thus obtained after rotating the system gives the loci of points where a principal direction makes a constant angle with a fixed reference axis equal to the angle of rotation of the polarizer and analyzer. This angle is referred to as an isoclinic parameter. In practice, isoclinic patterns are obtained for a number of parameters to give a composite picture and thus the direction of principal stresses at any point in the entire model can be found.

E.5 Stress Trajectory

Isoclinics, however, do not give direct information regarding the stress directions. This is better represented by a graphical construction derived from isoclinics and is known as the stress trajectory. The stress trajectories are the lines parallel or normal to the two principal stress directions at all points through which they pass. It is obvious then that free boundaries of the model are stress trajectories.

E.6 White Light Illumination

Relation (E.10) describes stress optic law as

$$\Delta = \frac{2\pi}{\lambda} h c (\sigma_1 - \sigma_2) \qquad (E.10)$$

This shows that the relative retardation Δ of the emerging rays is a function of light wavelength λ. White light consists of all wavelengths, hence constructive and destructive interference results for different values of $(\sigma_1 - \sigma_2)$. Each wavelength, therefore, displays its own intensity pattern in its own colour. This results in a colourful fringe pattern.

The human eye can interpret these white light fringe patterns accurately, since the eye can discern variation in colour with greater sensitivity than it can detect maximum or minimum intensity points. The photographic film, however, does not react as favourably to the white light fringe pattern, because the film tends to integrate all the colours, resulting in a wide band with relatively less sharply defined boundaries.

The white light fringe patterns are not normally used in an accurate photoelastic analysis since the polariscope requires the use of the so-called quarter wave plates which can, of course, produce quarter wave retardation for only one wavelength; in this case for green light at 5460 angstrom

wavelength. Any retardation for other wavelengths, particularly the extremes of blue and red, are not precise, causing a non linear effect. As the fringe order increases, the non linear effect is sufficient to "wash out" the resulting fringes making it impossible to interpret the results. Because the light source in this investigation (which is typical of others used in such analyses) was marginal in intensity, it was impossible to filter out the other wavelengths, hence results were not obtained at fringe orders higher than four.

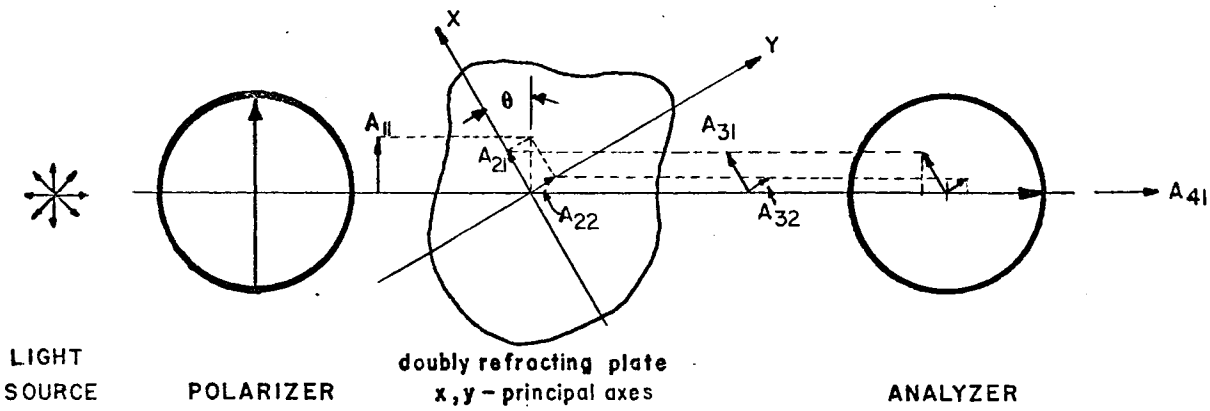

Figure E-1 - Arrangement of the various elements of a plane polariscope

VITA

1944 Born in Lalitpur, U.P., India

1965 Received the degree of Bachelor of Science in Mechanical Engineering from Banaras Hindu University, Varanasi, U.P. India

1967 Presently a candidate for the degree of Master of Applied Science in Mechanical Engineering at the University of Windsor, Windsor, Ontario, Canada